Title (12 words; 93 characters with spaces)

Bone marrow adipocytes drive the development of tissue invasive Ly6C^{high} monocytes during obesity

Running Title: Bone marrow fat linked to Ly6C^{high} monocytes in obesity

Parastoo Boroumand[1,2], David Prescott[3,4], Tapas Mukherjee[3], Philip J. Bilan[1], Michael Wong[1], Jeff Shen[1], Ivan Tattoli[4], Yuhuan Zhou[1], Angela Li[3], Tharini Sivasubramaniyam[3], Nancy Shi[1], Lucie Y Zhu[1], Zhi Liu[1], Clinton Robbins[3], Dana J. Philpott[3], Stephen E. Girardin[3,4], Amira Klip[1,2*].

[1]Cell Biology Program, The Hospital for Sick Children, Toronto, Ontario, M5G 0A4; Canada;

[2]Department of Biochemistry, University of Toronto, Toronto, Ontario, M5S 1A8; Canada;

[3]Department of Immunology, University of Toronto, Toronto, Ontario, M5S 1A8; Canada;

[4]Department of Laboratory Medicine and Pathophysiology, University of Toronto, Toronto, Ontario, M5S 1A8; Canada

*Corresponding Author:

Amira Klip, Ph.D.

Cell Biology Program

Hospital for Sick Children

Toronto, Ontario M5G 0A4, Canada

Phone: 416-813-6392

E-mail: amira@sickkids.ca

Summary (150 Words, 150):

During obesity and high fat-diet (HFD) feeding in mice, sustained low-grade inflammation includes not only increased pro-inflammatory macrophages in the expanding adipose tissue, but also bone marrow (BM) production of invasive Ly6C^{high} monocytes. As BM adiposity also accrues with HFD, we explored the relationship between the gains in BM white adipocytes and invasive Ly6C^{high} monocytes *in vivo* and through *ex vivo* paradigms. We find a temporal and causal link between BM adipocyte whitening and the Ly6C^{high} monocyte surge, preceding the adipose tissue macrophage rise during HFD. Phenocopying this, *ex vivo* treatment of BM cells with conditioned media from BM adipocytes or from *bona fide* white adipocytes favoured Ly6C^{high} monocyte preponderance. Notably, the switch towards the Ly6C^{high} subset was preceded by monocyte metabolic reprogramming towards glycolysis, reduced oxidative potential and increased mitochondrial fission. In sum, short-term HFD changes BM cellularity, resulting in local adipocyte whitening driving a gradual increase and activation of invasive Ly6C^{high} monocytes.

Keywords:

Obesity; Immunometabolism, Bone marrow monocytes, Bone marrow adipocytes, Tissue invasive monocytes, Ly6C^{high} monocytes, Glycolytic shift.

40 **Introduction**

41 A continuum of chronic obesity leading to metabolic disorders such as insulin resistance and
42 eventually type 2 diabetes is of paramount concern worldwide (Centers for Disease Control and Prevention,
43 2017; Hamann, 2017; WHO, 2016). An important contributor to the development and exacerbation of
44 insulin resistance is a gain in macrophages in adipose tissue (AT) (Liu et al., 2019; Weisberg et al., 2003),
45 muscle (Fink et al., 2014; Garvey et al., 2008) and liver (Lanthier et al., 2010) as well as their enhanced
46 pro-inflammatory (Lumeng et al., 2007, 2008; De Souza et al., 2005) and glycolytic switch (Sharma et al.,
47 2020). This low-grade inflammation is partly explained by circulating monocyte infiltration into tissues
48 where they differentiate to pro-inflammatory macrophages (Kohyama et al., 2016).

49 Ly6C^{high} monocytes in mice, and classical CD14^{++} CD16^{-} monocytes in humans, constitute the
50 predominant tissue-infiltrating monocyte subset during chronic inflammation. These tissue-invasive
51 monocytes are classified by high surface abundance of the Ly6C protein, the chemokine receptor CCR2
52 and the adhesion molecule L-selectin, all of which allow for monocyte extravasation from the BM and
53 infiltration into the tissues (Auffray et al., 2007; Boniakowski et al., 2018; Fink et al., 2014; Geissmann et
54 al., 2003; Weisberg et al., 2006). With obesity, the development of Ly6C^{high} monocytes along with their
55 stem and progenitor cells in the BM is boosted (Griffin et al., 2018; Manicone et al., 2016; Singer et al.,
56 2014) leading to a rise in available circulating Ly6C^{high} monocytes for tissue-infiltration (Friedrich et al.,
57 2019; Singer et al., 2014).

58 Various obesity-driven factors amalgamate for greater Ly6C^{high} monocyte infiltration into the AT
59 including (a) increased AT-dependent chemoattraction (Kamei et al., 2006; Nagareddy et al., 2014; Nov et
60 al., 2013; Renovato-Martins et al., 2017) and (b) enhanced BM myelopoiesis (Griffin et al., 2018; Manicone
61 et al., 2016; Singer et al., 2014). However, it is not clear whether the obesity-induced BM myelopoiesis
62 occurs prior to, concurrently, or after the elevation of AT macrophages. Since the BM is a highly-
63 vascularized tissue, home to hematopoietic and mesenchymal lineages, and is dynamically reactive to
64 environmental changes, we reasoned it might be an early responder to HFD-induced obesity, producing
65 increased Ly6C^{high} monocytes prior to their accumulation in the AT. Further, since BM-resident adipocytes

66 undergo hyperplasia and hypertrophy during obesity (Boroumand and Klip, 2020; Doucette et al., 2015;
67 Scheller et al., 2015; Tratwal et al., 2020) we contemplated that this process might be temporally and
68 potentially causally related to the HFD-driven BM myelopoiesis and Ly6C^{high} monocytosis. Finally, we
69 considered whether the response of the monocytic lineage to the BM environment during obesity includes
70 a metabolic shift leading to the increase in Ly6C^{high} monocytes. In fact, and surprisingly, little is known
71 about the metabolic orientation of the Ly6C^{high} monocytes in states of obesity, although there is mounting
72 evidence of a link between a macrophage-intrinsic metabolic shift and their pro-inflammatory orientation
73 in this condition (O'Neill et al., 2016; Sharma et al., 2020; Thapa and Lee, 2019; Verdeguer and Aouadi,
74 2017).

75 Hence, the overall hypothesis driving this study is that, with obesity, the increased production of
76 Ly6C^{high} monocytes in the BM is accompanied and possibly caused by a glycolytic shift in these cells,
77 driven by changes in bone marrow adipocytes (BMA). Accordingly, we investigated the temporality of
78 enhanced BM myelopoiesis, BM Ly6C^{high} monocyte accumulation, and AT macrophage accrual during
79 high fat diet (HFD) feeding in mice. Next, we explored the potential for a causal relationship between the
80 obesity-induced changes in BMA and increased Ly6C^{high} monocyte production. Using an *in vitro* platform,
81 we deconstructed the effects of obesity-induced BM cellular changes on Ly6C^{high} monocyte expansion. We
82 report that BM Ly6C^{high} monocytes accumulate in the BM prior to the gain in pro-inflammatory AT
83 macrophages. The rise in BM monocytes temporally correlated with the elevation in BMA. Moreover,
84 BMA whitening correlated with the timely increases in BM Ly6C^{high} monocytes, and remarkably, isolated
85 BMA from HFD-fed mice directly prompted Ly6C^{high} monocyte development *ex vivo*. This monocyte
86 developmental cue was also induced *ex vivo* by *bona fide* white adipocytes, while *bona fide* brown
87 adipocytes favoured Ly6C^{low} monocyte predominance. Noteworthy, the white adipocyte-induced swap in
88 proportion of Ly6C^{low} relative to Ly6C^{high} monocytes was preceded by a switch in monocyte metabolism
89 from oxidative to glycolytic. Mechanistically, brown adipocytes increased Ly6C^{low} monocyte proliferation
90 while white adipocytes appear to promote Ly6C^{low} monocyte conversion and potentially progenitor
91 expansion to increase Ly6C^{high} preponderance. We propose that HFD-induced changes in BMA disrupts

92 the normal balance of BM monocyte subsets leading to a higher output of tissue invasive Ly6C^{high}
93 monocytes.
94

95 **Results**

96 **Increased fasting blood glucose, peripheral and BM adiposity by 3 weeks of HFD**

97 To study the temporal relationship of HFD-induced myeloid changes in the BM relative to that in
98 epididymal white AT (EWAT), C57BL/6 mice were fed HFD or control low fat diet (LFD) for either 3, 8
99 or 18 weeks. HFD-fed mice had higher body weight and impaired fasting blood glucose by 3 weeks,
100 compared to controls (**Figure 1A,B**). Body weight and hyperglycemia continued to rise with prolonged
101 feeding. HFD-fed mice also displayed higher EWAT weight (**Figure 1C**) and inter-scapular brown AT
102 (BAT) weight at 3 weeks (not shown). Cross-sectional tibia and femur bone histology visualized via H &
103 E and Oil Red O staining revealed an increase in BMA size by 3 weeks and an increase in BMA number
104 by 8 weeks of HFD (**Figure 1D-G**). This indicated that 3 weeks of HFD sufficed to induce whole body
105 metabolic disturbance and augmented adiposity in peripheral tissues and in the BM.

106 **BM monocytes increase prior to accumulation of EWAT macrophages and monocytes with HFD**

107 Although total EWAT weight increased by 3 weeks, myeloid cells in the stromal vascular fraction
108 (SVF) of AT were not elevated until 8 weeks of HFD, as revealed by gene expression of the general myeloid
109 marker *Itgam* (encoding CD11b) and monocyte markers $Gr1^-$ $CD115^+$ $CD11b^+$ $Ly6C^+$ (determined by flow
110 cytometry) (**Figures 2A,D**). Similarly, AT macrophages, assessed by gene expression of the AT
111 macrophage marker *Adgre1* (encoding F4/80) and by flow cytometry counting of $CD11b^+$ $Ly6C^-$ $F4/80^+$
112 macrophages in the SVF were not elevated at 3 weeks of HFD but were at 8 weeks (**Figure 2B,E**). Further,
113 gene expression of the pro-inflammatory myeloid marker *Itgax* (encoding CD11c) and surface detection of
114 the pro-inflammatory markers $CD11b^+$ $Ly6C^-$ $F4/80^+$ $CD11c^+$ were also higher in the SVF by 8 weeks of
115 HFD relative to control diet, but not at 3 weeks (**Figure 2C,F**). Of note, gene expression of the
116 embryonically-conserved tissue-resident AT macrophage markers *Timd4* and *Marco* (Beattie et al., 2016;
117 Gibbings et al., 2015) was not elevated at 3 or at 8 weeks and only rose at 18 weeks of HFD (**Figure 2G-**
118 **H**). This indicates that the gain in AT macrophages at 8 weeks of HFD is unlikely due to proliferation of
119 resident macrophages and instead likely results from monocyte recruitment from the circulation.

120 In the BM, total monocytes, gated via the Gr1$^-$ CD115$^+$ CD11b$^+$ Ly6C$^+$ markers, increased at 3
121 weeks and continued to rise by 8 and 18 weeks of HFD (**Figure 2I**). Using the surface abundance of the
122 Ly6C protein as well as the CX3CR1 and CCR2 markers (Auffray et al., 2007, 2009; Kratofil et al., 2017),
123 we subcategorized Ly6C^{low} and Ly6C^{high} monocyte subsets. The two populations were identified by FACS
124 analysis using the gating strategy illustrated in Figure S1. At 3 weeks into the feeding study, Ly6C^{low} and
125 Ly6C^{high} monocytes represented about 40% of the total BM monocyte population in the control diet group,
126 whereas HFD promoted a higher proportion of Ly6C^{low} monocytes (**Figure 2J**). However, by 8 weeks of
127 HFD there was a marked shift, whereby the relative proportion of Ly6C^{low} monocytes in the total monocyte
128 population was *lower* and that of Ly6C^{high} monocytes was *higher* than under the control diet (**Figure 2J**).
129 These differences were more prominent by 18 weeks of HFD feeding (**Figure 2J**). Collectively, these
130 findings revealed that, in the BM, HFD favoured monocytosis at 3 weeks, with a subsequent and prominent
131 switch towards tissue invasive Ly6C^{high} monocytes at 8 weeks that continued into 18 weeks of HFD. Singer
132 et al. also demonstrated an increase in BM monocytosis and elevated monocyte progenitor cells with 18
133 weeks of HFD, that persisted after BM transplantation into chow-fed recipients (Singer et al., 2014). In the
134 present study, while we clearly recorded an earlier and continuing rise in total monocytes in HFD-fed mice
135 (**Figure 2I**), we did not observe statistically significant increases in monocyte progenitor and stem cells at
136 any time point analyzed (**Figure S2A-C**).

137 **Glycolytic metabolic reprograming in monocyte subsets with HFD**

138 Recent discoveries have highlighted the importance of glycolytic metabolism in the activation of
139 AT macrophages with HFD (Lee and Murphy, 2019), but the metabolic status of monocytes in obesity has
140 not been reported, although some studies have investigated the metabolism of circulating human
141 CD14$^+$CD16$^-$ monocytes (homologous to murine tissue invasive Ly6C^{high} monocytes) during aging (Lee
142 and Murphy, 2019; Pence and Yarbro, 2019). To assess whether HFD affects the metabolic status of BM
143 monocyte subsets in obesity we analyzed Ly6C^{low} and Ly6C^{high} from control and HFD mice at 3, 8 and 18
144 weeks of feeding. The mitochondrial activity-indicator dye MitoTracker Red CMXRos was incorporated

145 into the monocyte flow cytometry panel. MitoTracker Red CMXRos is recruited to the mitochondrial
146 membrane proportionally to the degree of mitochondrial membrane potential and is thus an indicator of
147 mitochondrial activity in oxidative phosphorylation. The results revealed that Ly6C^{low} monocytes have a
148 higher mitochondrial membrane potential than Ly6C^{high} monocytes in the control mice (**Figure 3A-C**).
149 Strikingly, 3 weeks of HFD reduced the mitochondrial membrane potential in both monocyte subsets
150 indicated by the left-ward shift in the MitoTracker Red CMXRos peak (**Figure 3A**). The HFD-induced
151 effects were more pronounced by 8 and 18 weeks of HFD (**Figure 3B,C**). To further understand the effects
152 of HFD on the developing BM monocytes, Ly6C^{low} and Ly6C^{high} monocytes from mice fed control or HFD
153 for 3, 8 or 18 weeks were isolated via fluorescent activated cell sorting (FACS) and plated for metabolic
154 analysis with a Seahorse XF Analyzer. The results revealed a gradual lowering in the oxygen consumption
155 rate (OCR) of Ly6C^{low} monocytes with HFD (**Figure 3D-I**). Comparison of the area under the curve (AUC)
156 revealed that at 18 weeks, the OCR of the Ly6C^{low} monocytes was significantly lowered with HFD (**Figure**
157 **3I**). Interestingly, at 8 and 18 weeks, the AUC of the OCR of the Ly6C^{low} monocytes was significantly
158 higher than the AUC of the OCR of Ly6C^{high} monocytes in the control group (**Figure 3H-I**). Moreover, this
159 difference was lost in the HFD group as the AUC of the OCR of Ly6C^{low} monocytes diminished (**Figure**
160 **3H-I**).

161 Comparison of the various sections of the OCR graph revealed that the changes in OCR observed
162 with 3 weeks of HFD were not manifest at basal respiration nor at the ATP-dependent respiration, rather
163 they were evident in the maximal respiratory capacity portion of the metabolic stress test (**Figure 3D**). A
164 drop in basal respiration of both monocyte subsets emerged with 8 weeks of HFD and became more
165 pronounced with 18 weeks of HFD (**Figure 3E-F**). This showcased the sustained effects of HFD on
166 monocyte metabolic status. Conversely, the extracellular acidification rate (ECAR) of Ly6C^{low} monocytes
167 was higher than that of Ly6C^{high} monocytes, consistent with a more active metabolism in the former (**Figure**
168 **3J**). However, this difference was lost with HFD, as ECAR dropped in the Ly6C^{low} monocytes and rose in
169 the Ly6C^{high} monocytes relative to the control diet group (**Figure 3J**). Overall, these results suggest that,

170 along with promoting the preponderance of Ly6C^{high} monocytes, HFD also lowers OCR in Ly6C^{low}
171 monocytes.

172 Endorsing these findings, an analysis of the BM revealed elevated lactate levels across all HFD
173 time points (**Figure 3K**). This increase in lactate may be due to the glycolytic shift in BM monocytes
174 described above, among other potential sources within the BM cellular composition. Further analysis of the
175 BM soluble fraction failed to evince any changes between control and 18-week HFD-fed mice in pro-
176 inflammatory cytokines TNFα, IL-1β, IL-6, CXCL1 or CCL2 (**Figure S3A-C**). Similarly, there were no
177 differences between diet groups in pro-inflammatory gene expression of *IL-6*, *IL-1β* or *Itgax* in FACS-
178 sorted Ly6C^{low} and Ly6C^{high} monocytes (Not Shown). However, *TNFα* gene expression was higher in
179 FACS-sorted Ly6C^{high} monocytes from 18-week HFD-fed mice compared to controls (**Figure S3D**).
180 Collectively, these findings reveal that HFD alters the BM metabolic micro-environment with little effect
181 on pro-inflammatory cytokine secretion (based on the panel tested).

182 **Expression of mitochondrial fusion and fission genes in monocytes is altered by HFD**

183 The efficiency of mitochondrial function is largely reliant on its structure. Mitochondria are highly
184 dynamic in structure, largely regulated by concentration of proteins that control fission and fusion (Gottlieb
185 and Bernstein, 2017). Dynamic transitions are closely aligned to metabolic performance. To further assess
186 the mitochondrial activity of monocytes, we enquired whether their expression of mitochondrial dynamic
187 genes is altered with HFD compared to the control group.

188 The analyzed genes involved in mitochondrial fusion were *Mfn1*, *Mfn2*, *Opa1*, *Tomm20* and
189 *Tomm40*, while those involved in mitochondrial fission were *Drp1*, *CypD* and *Fis1*. BM monocytes from
190 mice fed HFD for 3 weeks did not present with differences in gene expression in the tested mitochondrial
191 fusion genes compared to control diet counterparts (**Figure 4A**). BM monocytes isolated from mice fed
192 HFD for 8 weeks showed downregulated *Mfn1* and *Mfn2* compared to the controls (**Figure 4B**). BM
193 monocytes isolated from 18-week HFD-fed mice downregulated the mitochondrial fusion genes *Mfn2*,
194 *Opa1*, and *Tomm20* (**Figure 4C**). Furthermore, from the tested mitochondrial fission genes, *Drp1* was

195 upregulated in the BM monocytes of 3 weeks HFD-fed mice (**Figure 4D**). *Drp1* and *CypD* were also
196 upregulated in BM monocytes of 8 weeks HFD-fed mice (**Figure 4E**). At 18 weeks, all three tested
197 mitochondrial fission genes, *Drp1*, *CypD* and *Fis1* were upregulated (**Figure 4F**). This gene expression
198 pattern suggests that HFD changes the monocyte gene expression to favour downregulation of genes
199 involved in mitochondrial fusion and upregulation of genes involved in fission.

200 Given that Ly6C^{low} and Ly6C^{high} monocytes presented with differences in metabolic preference
201 (glycolytic and oxidative, respectively), and the known link of glycolytic metabolism with mitochondria
202 fragmentation and conversely oxidative metabolism to mitochondrial fusion, we assessed whether the
203 expression patterns of the genes governing mitochondrial fission and fusion would correlated distinctly
204 with the BM monocyte subset abundance in control and HFD-fed mice. Indeed, and notably, the abundance
205 of the Ly6C^{high} monocyte subset negatively correlated with *Mfn2* and positively correlated with *Drp1* levels
206 (**Figure 4G-H**). In contrast, the abundance of BM Ly6C^{low} monocytes did not correlate with the expression
207 patterns of either *Mfn2* or *Drp1* (**Figure 4G-H**). These data are consistent with our metabolic findings
208 suggesting Ly6C^{high} monocytes are more glycolytic and adopt a gene expression pattern that would promote
209 mitochondrial fragmentation.

210

211 **A shift in BMA type at 8 weeks of HFD influences monocyte subset preference and mitochondrial**
212 **dynamic gene expression**

213 Hematopoietic myeloid cells reside in specific niches of the BM that determine their cellular
214 interaction with other co-resident BM cells (Boroumand and Klip, 2020). BMA, while representing a unique
215 type of adipocytes, respond to obesity with an increase their white adipocyte-like fat storing properties and
216 a decrease in brown-like characteristics (Ambrosi et al., 2017; Doucette et al., 2015; Krings et al., 2012;
217 Scheller et al., 2016). To explore the temporal relation of BMA whitening in relation to the development
218 of monocyte subsets, we followed the gene expression of a suite of recently identified markers that are good
219 differentiators of adipocyte types (Nascimento et al., 2014; Ussar et al., 2014) in isolated BMA from femur

220 and tibia of control and HFD-fed mice. By 3 weeks into HFD, the white adipocyte marker Asc1 (encoding
221 the guanine nucleotide-binding protein subunit beta-like protein) was significantly higher and the brown
222 adipocyte marker P2rx5 (encoding purinergic receptor P2X) trended to be lower albeit without reaching
223 statistical significance, relative to control diet. White adipocyte markers *Lep* (leptin) and *AdipoQ*
224 (adiponectin) as well as the brown adipocyte markers *Ucp1* (UCP1) and *Pat2* (Integrin alpha pat-2) did not
225 change (**Figure 5A**). By 8 weeks of HFD, *Asc1* mRNA remained elevated and *Lep* and *AdipoQ* trended in
226 the same direction (**Figure 5B**). Brown adipocyte markers *P2rx5* and *Ucp1* in the isolated BMA of HFD
227 mice were markedly lower relative to those from control diet mice (**Figure 5B**). Thus, 8 weeks of HFD
228 sufficed to shift BMA towards white adiposity. By 18 weeks of HFD, all white adipocyte markers genes
229 showed were upregulated while brown adipocyte markers were downregulated compared to the control
230 group (**Figure 5C**). Analyses of adipocyte differentiation and progenitor cell markers were conducted in
231 the BM pelleted fraction. *Hoxc8*, a regulator of adipocyte progenitors (Nakagami, 2013), was significantly
232 upregulated at 8 weeks along with *Hoxc9* at 18 weeks of HFD (**Figure S4B,C**). The beige adipocyte
233 progenitor marker *Tmem26* was not significantly higher at any of the tested HFD durations (**Figure S4A-**
234 **C**). Expression of the brown adipocyte determinant genes *Tbx1* and *Lhx8* was undetectable in the isolated
235 BMA. Thus, during the course of HFD, while markers for white adipocyte progenitor cells were
236 upregulated, precursors of beige/brown adipocytes were not affected.

237 The rise in BM Ly6C^{high} monocytes and the shift in BMA whitening both manifested by 8 weeks
238 of HFD. Correlative analysis was performed for both Ly6C^{low} and Ly6C^{high} with the white adipocyte marker
239 *Asc1* and the brown adipocyte marker *Ucp1*. The results revealed a significant positive correlation (P value
240 of 0.0123) for Ly6C^{high} monocytes with *Asc1* gene expression (**Figure 5D**). Conversely, the surge in
241 Ly6C^{high} monocytes presented a significant negative correlation (P value of 0.0415) relative to *Ucp1* gene
242 expression (**Figure 5E**). Changes in Ly6C^{low} monocytes did not significantly correlate with *Asc1* (P value
243 of 0.0768) or *Ucp1* (P value of 0.1299) (**Figure 5D-E**). Collectively, the above data suggest the possibility
244 that the mere shift in BMA towards white adiposity may directly favour induction of BM Ly6C^{high}
245 monocytes. To test this hypothesis, we generated conditioned media (CM) from BMA (BMA-CM) pooled

246 from three control and three HFD-fed mice, collected 3, 8 and 18 weeks into the diets. In parallel, BM of
247 control mice was used to generate monocytes through a 5-day *in vitro* differentiation protocol (as reported
248 by (Francke et al., 2011), see Methods). These monocytes were treated with BMA-CM from control and
249 HFD-fed mice for 18 h thereafter. Subsequently, the monocyte population was analyzed via flow cytometry.
250 BMA-CM from 3 weeks HFD-fed mice had no effect on the monocyte subset proportions compared to
251 BMA-CM from control diet-fed mice (**Figure 5F**). Strikingly, however, BMA-CM from 8-week HFD-fed
252 mice applied to BM-derived monocytes from control mice resulted a significant production of Ly6C^{high}
253 monocytes compared to the effect of BMA-CM from mice on the 8-week control diet (**Figure 5G**). This
254 skewing was further enhanced when exposing the control BM cells to BMA-CM from 18-week HFD-fed
255 mice (**Figure 5H**).

256 Lastly, we tested whether BMA-CM was capable to induce changes in gene expression of the
257 mitochondrial fusion and fission genes in monocytes, as observed with monocytes isolated from HFD-fed
258 mice. Accordingly, *in vitro*-generated monocytes were treated with BMA-CM from control and HFD-fed
259 mice. As before, the analyzed genes involved in mitochondrial fusion were *Mfn1*, *Mfn2*, *Opa1*, *Tomm20*
260 and *Tomm40*, while the tested genes involved in mitochondrial fission were *Drp1*, *CypD* and *Fis1*.
261 Monocytes treated with BMA-CM from HFD-fed mice for 18 weeks showed significant downregulated
262 mitochondrial fusion genes *Mfn2*, *Tomm20* and *Tomm40* (**Figure 5I**). Conversely, the mitochondrial fission
263 genes *Drp1* and *CypD* were significantly up-regulated in monocytes treated with HFD-derived BMA-CM
264 (**Figure 5J**).

265 These results not only show that HFD-derived BMA-CM can bias monocyte subset cellularity but
266 also can alter mitochondrial morphology via changes in mitochondrial dynamic gene expression. These
267 changes can have consequential effects on the metabolic properties on the monocytes.

268 **White adipocytes favour Ly6C^{high} monocytes and promote mitochondrial fragmentation**

269 To assess whether the effects of BMA on monocyte subset skewing and metabolic differences can
270 be attributed to BMA whitening, we designed a proof-of-concept experiment studying the influence of *bona*

271 *fide* white or brown adipocytes on monocyte subset determination and metabolic changes *ex vivo*. Isolated
272 adipocytes from EWAT and brown adipocyte tissue (BAT) of three mice were pooled to generate white AT
273 adipocytes (WATA) and brown AT adipocytes (BATA), respectively. Confirming the phenotype of the
274 isolated cells, classical white adipocytes markers were solely expressed in the isolated WATA, and classical
275 brown adipocyte markers were exclusively expressed in the BATA (**Figure S4D-E**). The isolated WATA
276 and BATA were cultured for 24 h and the corresponding CM were collected for subsequent treatment of
277 monocyte preparations. *In vitro*-generated BM-derived monocytes from chow-fed mice were treated with
278 WATA-CM, BATA-CM or left untreated. The proportion of Ly6C^{low} and Ly6C^{high} monocyte subsets was
279 determined by flow cytometry analysis (**Figure S1**). This *in vitro* paradigm allowed for direct mechanistic
280 analysis of the influence of white or brown adipocytes on monocytes. These results indicate that WATA-
281 CM favoured Ly6C^{high} monocyte predominance, while BATA-CM prompted Ly6C^{low} monocyte abundance
282 (**Figure 6A-B**), revealing a novel, differential influence of white and brown adipocytes on monocyte
283 orientation preference. Similarly, CCR2 surface receptors also increased in the monocytes incubated with
284 WATA-CM (Not Shown), validating the effects of white adipocytes in promoting an abundance of tissue
285 invasive Ly6C^{high} monocytes.

286 Since segregated Ly6C^{low} and Ly6C^{high} monocyte subsets had different metabolic orientations, we
287 investigated if the differential adipocyte influence on monocyte subset development corresponded to a
288 change in their metabolic status. To this end, *in vitro*-generated monocytes were treated with WATA-CM,
289 BATA-CM or left untreated for the last 18 h of the monocyte differentiation protocol. The mitochondrial
290 membrane potential was assessed using MitoTracker Red CMXRos and flow cytometry analysis.
291 Remarkably, Ly6C^{low} monocytes incubated *in vitro* with WATA-CM experienced a left-ward shift in
292 MitoTracker Red CMXRos peak revealing a reduction in mitochondrial membrane potential induced by
293 the WATA-CM (**Figure 6C**), reproducing what was observed with monocytes from HFD-fed mice (see
294 **Figure 3A-C**). Furthermore, the gene expression of mitochondrial fusion genes *Mfn1*, *Mfn2*, *Tomm20* and
295 *Tomm40* were reduced in monocytes treated with WATA-CM (**Figure 6D**). The mitochondrial fission
296 genes *Drp1*, *CypD* and *Fis1* were up-regulated in monocytes treated with WATA-CM (**Figure 6E**).

297 Conversely, treating monocytes with BATA-CM downregulated the mitochondrial fission gene *CypD*
298 (**Figure 6E**). To explore if the changes in mitochondrial fusion and fission gene expression correlated
299 with the corresponding mitochondrial morphology, we utilized super-resolution microscopy to image the
300 mitochondrial protein TOM20 in *in vitro* monocytes adhered to coverslips.

301 WATA-CM induced a striking increase in the percentage of cells with fragmented mitochondria,
302 from 22% in control CM-treated cells to 64%. On the other hand, BATA-CM raised mitochondrial
303 elongation from 20% in CM-treated cells to 55% (**Figure 6F-H**). These observations suggest that white
304 adipocyte products alter the metabolic status of Ly6C^{low} monocytes by reducing their mitochondrial
305 membrane potential and altering mitochondrial dynamic gene expression and morphology, thereby
306 linking changes in BMA whitening to monocyte metabolic status. Moreover, the shift to mitochondrial
307 fragmentation coincided with the higher abundance Ly6C^{high} monocytes resulting from in vitro-generated
308 monocytes with WATA-CM (**Figure 6A,B**).

309 **White and brown adipocytes influence monocytes through distinct mechanisms**

310 Monocyte precursor cells in the BM in the tissues maintain cell numbers by cell proliferation
311 (Cassado et al., 2015). Although we had not detected HFD-induced changes in hematopoietic stem and
312 monocyte progenitor cells *in vivo*, we assessed the abundance of these progenitor cell populations upon
313 exposing *in vitro*-generated monocytes to WATA-CM and BATA-CM. We reasoned that the *ex vivo*
314 experimental setup lent itself well to gain understanding of the mechanisms whereby monocytes undergo
315 changes in subset proportion in response to *bona fide* white and brown adipocyte media. The abundance of
316 hematopoietic stem and monocyte progenitor cells was determined using appropriate surface markers and
317 flow cytometry analysis (**Table 1, Figure S1D**). A small gain in myeloid progenitor cell (CMP) was
318 observed in response to WATA-CM treatment (**Figure S5A-C**). However, no differences in the abundance
319 of CD117+, Sca1+, Sca1-, and GMP cells were detected (**Figure S5A-C**). GMP cells are downstream of
320 CMP during lineage progression of progenitor cells towards monocytes or erythroid cells (Yáñez et al.,

321 2017), and so it is noteworthy these cells did not become more abundant with WATA-CM treatment, even
322 though content of CMP, their upstream multipotential progenitors, was slightly elevated.

323 Next, we asked whether proliferation might contribute to the higher proportion of terminally
324 differentiated Ly6C^{high} or Ly6C^{low} monocyte subsets observed following treatment with WATA-CM (in
325 addition to the conversion of Ly6C^{low} into Ly6C^{high}) or BATA-CM, respectively. To this end, we treated
326 BM-derived *in vitro*-generated monocytes with WATA-CM, BATA-CM or left them untreated for 18 h,
327 with or without the presence of bromodeoxyuridine (BrdU), an indicator of S-phase. Using flow cytometry
328 analysis, DNA-incorporated BrdU was detected in the Ly6C^{low} or Ly6C^{high} monocyte gates of the CD11b
329 versus Ly6C plots, with BrdU as the third colorimetric axis. Although at the highest levels the CD1b signal
330 created a green background signal in the BrdU channel (as seen in samples not treated with BrdU), the
331 actual BrdU signal could be readily distinguished by the yellow to red signal corresponding to the illustrated
332 gradient scale shown. Proliferating cells were quantified as percentage of CD11b^{+} Ly6C^{+} cells that were
333 positive for BrdU incorporation (yellow to red signal). WATA-CM-treated monocytes rendered the
334 expected increase in Ly6C^{high} monocytes, yet these cells did not show any significant incorporation of BrdU,
335 implying that they are not actively replicating their DNA. In contrast, BATA-CM increased DNA-
336 incorporated BrdU in the sorted Ly6C^{low} monocyte subset, visualized as yellow to red hues in the CD11b^{+}
337 Ly6C^{low} cell gate (**Figure 7A**), and the number of proliferating cells was elevated by 25-fold (**Figure 7B**).
338 These findings revealed that brown adipocytes promote an abundance of Ly6C^{low} monocytes by inducing
339 their proliferation. Interestingly, this replicative behavior of BATA-CM-treated of Ly6C^{low} monocytes,
340 which we showed above are more oxidative than Ly6C^{high} monocytes, is consistent with recent findings
341 that proliferative cells have higher glucose consumption and oxidative phosphorylation relative to quiescent
342 cells (Yao et al., 2019).

343 To buttress the above results, we also assessed the colony forming potential of *in vitro*-generated
344 monocytes that received pre-treatment of WATA-CM or BATA-CM, to assess the potential for expansion
345 of progenitor cells present in the samples. Colonies were identified as BFU-E (giving rise to erythroid cells);
346 CFU-GEMM (giving rise to large mixed cultures of granulocyte, erythroid, macrophage, megakaryocyte;

347 also, known as CMP); CFU-G (giving rise to granulocytes) or CFU-M (giving rise to macrophages). BATA-
348 CM promoted growth of CMP/CFU-GEMM cultures over control Media (**p<0.01 Two-way ANOVA,
349 Tukey's multiple comparisons, **Figure 7C**) and biased granulocyte/macrophage progenitors (widely known
350 as GMP) towards macrophage over granulocyte differentiation, relative to control Media (**p<0.01) or
351 WATA-CM (*p<0.05 or ***p<0.001, **Figure 7C**). The total numbers of colonies that grew after 7-10 days
352 of culturing of each pre-treated cohort of monocytes were not different across the three treatments, although
353 trended upwards with BATA-CM (**Figure 7D**). These results revealed that while BATA-CM promoted
354 expansion of selected populations (CMP/CFU-GEMM and CFU-M), consistent with the increase in BrdU
355 incorporation shown above, WATA-CM was without effect relative to control Media.

356 The above findings suggest that while the proportional increase in Ly6C^{low} monocytes induced by
357 BATA-CM involves cell proliferation, the proportional increase in Ly6C^{high} monocytes induced by WATA-
358 CM does not. As a complementary approach, BM cells were analyzed by flow analysis for the presence of
359 monocyte progenitors within the Ly6C^{low} or Ly6C^{high} monocyte subsets. GMP progenitor cells were
360 essentially the only progenitors detected by this approach in the Ly6C^{low} monocyte subset, and they
361 represented 140 GMP per 1000 Ly6C^{low} cells (**Figure 7E**). During the incubation time of 18 h with
362 conditioned medium, we anticipate the progenitors could theoretically undergo only one doubling and
363 therefore unlikely to account for the overall changes in Ly6C^{low} cell numbers produced by WATA-CM.
364 The above findings indicate that WATA-CM treatment did not result in any appreciable expansion
365 of progenitor cells or colony formation. Accordingly, alternative mechanisms had to be explored that might
366 contribute to the WATA-CM induced shift towards Ly6C^{high} monocyte preponderance. It is known that
367 Ly6C^{high} monocytes give rise to Ly6C^{low} monocytes in mouse blood and BM, and this is paralleled by the
368 human homologous CD14 and CD16 monocyte subsets (Kratofil et al., 2017; Lessard et al., 2017; Patel et
369 al., 2017). However, while there has been speculation about the conversion of Ly6C^{low} to Ly6C^{high}
370 monocytes, there is little experimental evidence for this phenomenon. Hence, we contemplated the
371 possibility that BATA-CM may also cause Ly6C^{high} to Ly6C^{low} monocyte conversion, and especially

372 whether WATA-CM might cause Ly6C^{low} to Ly6C^{high} monocyte conversion, however unprecedented. To
373 this end, we collected each FACS-sorted, homogenous Ly6C^{low} and Ly6C^{high} monocyte populations and,
374 once isolated, treated them with WATA-CM, BATA-CM, or control media for 18 h. Following treatments,
375 we evaluated the presence of the alternative monocyte subtype relative to that in the respective starting
376 homogenous populations. Surprisingly, no conversion from Ly6C^{high} (red) to Ly6C^{low} (gray) monocytes
377 was observed in any condition (**Figure 8A-F**), but, remarkably, there was a switch of the FACS sorted
378 Ly6C^{low} population, as Ly6C^{high} monocytes became more prevalent following exposure to WATA-CM
379 (their proportion accounting to 49.7% of monocytes) (**Figure 8B,E**). This was in stark contrast to all other
380 isolated cell and CM treatment combinations tested, which gave rise to a maximum of 16.3% of the opposite
381 monocyte subset compared to the starting population. Taken together, the results from Figures 7 and 8
382 endorse the novel possibility of Ly6C^{low} into Ly6C^{high} monocyte conversion induced by secreted factors
383 from white adipocytes.
384

385 **Discussion**

386 In this study, we demonstrate a temporal correlation between HFD-induced whitening of BMA and
387 a BM myeloid lineage bias towards Ly6C^{high} monocytes *in vivo*. The latter present a more glycolytic
388 metabolism underpinned by a reduction in mitochondrial membrane potential, a rise in mitochondrial
389 fission genes and a reduction in mitochondrial fusion genes. Causatively, we show that CM from BMA of
390 HFD-fed mice promotes the generation of Ly6C^{high} monocytes *ex vivo.* Phenocopying the effect of BMA
391 derived from HFD-fed mice, *bona fide* WATA favoured a Ly6C^{high} monocyte preponderance, while BATA
392 promoted a dominance of Ly6C^{low} monocytes. Interestingly, these differential influences by the respective
393 adipocytes are induced by distinct cellular pathways. Mechanistically, white adipocytes induced a shift in
394 monocyte subset proportion, from Ly6C^{low} to Ly6C^{high} monocytes suggesting a novel conversion of one
395 subset into the other, while brown adipocytes favoured Ly6C^{low} predominance by inducing their
396 proliferation. These changes in monocytes were underpinned by alterations in monocyte metabolism, as
397 WATA blunted the monocytes' mitochondrial membrane potential and OCR. Overall, our findings reveal
398 a regulation of monocyte subsets directly influenced by adipocytes, whether from the BM or from AT.
399 Along with the observation of dynamic whitening of BMA during HFD, our results contribute to the
400 emerging evidence that BMA are not mere space fillers, rather they are important contributors to cellular
401 metabolism and hematopoietic lineage decisions (Boroumand and Klip, 2020). That these changes occur
402 early on in the course of diet-induced obesity suggests that the BM is an early responder to a change in
403 feeding status and that adipocytes play a significant role in directing monocyte subset skewing. Moreover,
404 they reveal novel mechanisms regulating the genesis of such skewing.

405 **BM as an early sensor and an active contributor to HFD-induced AT macrophage accumulation**

406 It is now widely recognized that many factors contribute to the accumulation of macrophages in
407 AT that includes the contribution of monocytes. There is mounting evidence for both HFD-induced EWAT
408 monocyte chemo-attraction and for enhanced BM myelopoiesis, that work together to increase the
409 monocyte infiltration and pro-inflammatory AT macrophage accumulation (Singer et al., 2014; Trottier et

410 al., 2012 and Fig. 1D-H). Singer et al. demonstrated that transplantation of BM from 18-week HFD-fed
411 mice into control recipients increased the number of invasive circulating monocytes and pro-inflammatory
412 AT macrophages (Singer et al., 2014). These pioneering findings heralded the notion that HFD influences
413 hematopoietic myeloid bias in the BM upstream of monocyte tissue invasion, thereby contributing to
414 downstream systemic and peripheral tissue inflammation. Furthermore, HFD-driven chemoattracting
415 signals from the homeostatically-disrupted EWAT initiate tissue influx and depletion of invasive Ly6C^{high}
416 monocytes from the circulation, which in turn may acts as a signal for their increased production in the BM
417 (Kamei et al., 2006; Nagareddy et al., 2014; Nov et al., 2013; Renovato-Martins et al., 2017).

418 In the present study, by analyzing chronological changes in EWAT and BM myeloid composition,
419 we observed that total BM monocytes increase by 3 weeks of HFD, whereas the proportion of Ly6C^{high}
420 monocyte predominance was evident only at 8 weeks coinciding with a gain in AT macrophages that were
421 also pro-inflammatory oriented. We did not observe statistical significance in HFD-dependent changes in
422 myeloid progenitors, likely due to their scarcity since HSC make up only 0.01% of the entire BM nucleated
423 cells (Challen et al., 2009). The rise in total monocytes observed at 3 weeks of HFD and prior to elevation
424 of AT macrophages identifies the BM as an earlier-responding *locus* during HFD. Interestingly, the increase
425 was only apparent in Ly6C^{low} patrolling monocytes and not in the Ly6C^{high} tissue invasive monocyte subset
426 that is known for tissue infiltration in chronic obesity. This might be explained by an initial non-specific
427 upregulation of total myelopoiesis and an increased Ly6C^{high} monocyte BM extravasation. Therefore, it
428 appears that only Ly6C^{low} monocytes are elevated in the BM at 3 weeks of HFD. By 8 weeks of HFD, we
429 observed a shift in the monocyte subset proportion, favouring Ly6C^{high} monocytes. Thus, by 8 weeks, the
430 BM has adopted the 'typical' HFD-induced hematopoietic phenotype, in so far as it already shows the
431 increased Ly6C^{high} monocytes previously reported at the habitually studied 16-18 weeks of HFD.
432 Importantly, we detected a gain in pro-inflammatory AT macrophages by 8 weeks of HFD that is concurrent
433 with the predominance of invasive Ly6C^{high} monocytes in the BM. In contrast, the embryonic-derived tissue
434 resident AT macrophage markers, *Timd4* and *Marco* (Beattie et al., 2016; Gibbings et al., 2015), were not

435 elevated until 18 weeks of HFD. This brings to light the importance of the contribution of the BM-derived
436 myeloid cell pool to early EWAT pathology and AT macrophage accumulation.

437 **Changes in BMA influence monocyte subset skewing**

438 BMA are distinctive components of the BM cellular suite that is sensitive to HFD effects (Pham et
439 al., 2020). In lean mice, BMA present characteristics that are similar to those of beige or brown adipocytes
440 in peripheral AT (Cuminetti and Arranz, 2019). With HFD, BMA undergo hyperplasia and hypertrophy
441 triggered by PPARγ activation (Rosen and MacDougald, 2006). Furthermore, with obesity, adipocyte
442 precursor mesenchymal stem cells tilt their lineage commitment towards adipogenesis (Silva et al., 2016,
443 Bowers and Singer, 2021). While BMA are now known to be a distinct adipocyte population, they express
444 several characteristics of white and brown adipocytes (Boroumand and Klip, 2020; Krings et al., 2012;
445 Sulston and Cawthorn, 2016; Tratwal et al., 2020). Brown adipocyte markers of BMA are reduced in obese
446 mice and a parallel adoption of more white adipocyte markers has been observed (Adler et al., 2014b;
447 Doucette et al., 2015; Krings et al., 2012). The amalgamation of upregulated white adipocyte proteins and
448 elevated fat storage capacity is known as BM adipocyte whitening. Obesity-induced gains in whole body
449 adiposity was causally linked to elevated circulating $CD11b^+$ monocytes (Takahashi et al., 2003). However,
450 the influence of BMA from either lean or obese mice on the expansion of $CD11b^+$ monocytes had not been
451 previously investigated.

452 The limited spatial capacity of the BM interior as well as the proximity of the cellular lineages in
453 the various BM niches lead us to anticipate that the obesity-linked BMA whitening would influence the
454 monocytic lineage. Here, we found a temporal, positive link between BMA hypertrophy and monocytosis
455 at 3 weeks of HFD. By 8 weeks of HFD, BMA whitening also positively correlated with the rise in tissue
456 invasive $Ly6C^{high}$ monocytes in the BM. We did not observe significant gains in progenitor cells (CMP,
457 GMP) at either 3, 8 or 18 weeks of HFD compared to control diet, whereas Singer et al. found these cells
458 elevated at 16 weeks of HF-feeding (Singer et al., 2014, Singer et al., 2015). However, in another study, at
459 4 weeks of HFD, they did not observe changes in progenitor populations (PMID: 25869128), when

460 monocyte skewing towards Ly6C^{high} phenotype was already observed, apparently dissociating the
461 progenitor proliferative potential from the change in proportion of this monocyte subset.

462 As proof-of-concept for a direct and distinctive influence of adipocytes on monocyte number and
463 subsets, we show that exposure to soluble factors from *bona fide* white adipocytes favours Ly6C^{high}
464 monocyte preponderance while exposure to soluble factors from brown adipocytes promotes the
465 preponderance of Ly6C^{low} monocytes. Mechanistically, we observed that white adipocytes induced a
466 change in the proportion of Ly6C^{low} towards Ly6C^{high} monocytes, an unprecedented process that is not well
467 understood at present. Although the Ly6C^{low} population contained some level of multipotential progenitor
468 cells, it is unlikely that these contribute in a major way to the switch in preponderance of Ly6C^{high}
469 monocytes in response to WATA-CM, since this population did not undergo changes in the proximal
470 lineage-committed precursors (CFU-M) when assayed for colony forming unit potential, and further did
471 not involve BrdU accrual (indicative of DNA replication and cell proliferation).

472 Brown adipocytes, on the other hand, induce their influence on Ly6C^{low} monocytes by increasing
473 their proliferation, evinced by promoting BrdU incorporation into monocytes and an inducing expansion of
474 monocyte lineage-committed precursor CFU-M colonies when tested for colony formation. Interestingly,
475 secretome studies have reported that BAT-derived VEGFA and VEGFB can stimulate proliferation in
476 adipocyte progenitors and endothelial cells (Bagchi et al., 2013; Leung et al., 1989). Adipocyte-specific
477 VEGFA transgenic mice were protected from the effects of HFD and presented altered macrophage
478 polarization (Elias et al., 2012). Therefore, it is conceivable that a reduction in brown adipocyte
479 characteristics of BMA also leads to a drop in the factors that would normally favour proliferation of
480 Ly6C^{low} monocytes. While the identification of the soluble unknown factor(s) responsible for the adipocyte-
481 specific myeloid influence is outside the focus of the present study, we have laid the foundation for a future,
482 comprehensive investigation of the molecular mediators involved.

483 **How do adipocytes skew myeloid lineage subsets?**

484 While the designation of macrophages as 'M1 and M2' (of pro- or anti-inflammatory
485 characteristics, respectively) represents the extremes of a wide spectrum of phenotypes, the 'M1' pro-
486 inflammatory orientation has been linked to glycolytic activation while the 'M2' anti-inflammatory
487 orientation has been linked to oxidative phosphorylation (Castoldi et al., 2016; Kelly and O'Neill, 2015).
488 A similar glycolytic metabolic switch with obesity has been reported for CD8 pro-inflammatory T cells
489 (Buck et al., 2017). Surprisingly, while pro-inflammatory pathways in monocytes are activated by
490 hyperglycemic conditions (Shanmugam et al., 2003), the metabolic preference of the different monocyte
491 subsets had not been explored. This is a compelling question, given that Ly6C^{high} monocytes penetrate
492 tissues and differentiate to pro-inflammatory 'M1' AT macrophages while Ly6C^{low} monocytes enter tissues
493 to promote healing and repair (Geissmann et al., 2003; Lin et al., 2009). Therefore, we hypothesized here
494 that, in the context of metabolic inflammation, there is a change in the metabolic phenotype of monocyte
495 subsets.

496 Our findings show that Ly6C^{high} and Ly6C^{low} monocytes had different metabolic preferences at
497 baseline, with Ly6C^{low} having higher mitochondrial membrane potential indicative of more active oxidative
498 phosphorylation. Interestingly, HFD consumption lowered the mitochondrial membrane potential of both
499 Ly6C^{low} and Ly6C^{high} monocytes, implicating a reduction in their mitochondrial oxidative capacity. This
500 change aligned with a HFD-induced reduction in oxygen consumption by Ly6C^{low} monocytes. Importantly,
501 this difference was observed as early as 3 weeks and exacerbated by 8 and 18 weeks of HFD. The elevated
502 lactate concentration measured in the BM at all HFD durations may be reflective of metabolic changes in
503 cells of the BM cavity. Since we did not observe changes in the lactate levels in WATA-CM or BATA-
504 CM, the higher lactate in BM of HFD-fed mice may not originate from changes in BMA.

505 Along with the change in monocyte subset proportions, we observed an increase in genes
506 responsible for mitochondrial fragmentation and a decrease in those involved in mitochondrial elongation
507 in monocytes from HFD-fed mice and treated with WATA-CM and BMA-CM. The physiological
508 consequence of these changes was revealed by the observation of a striking mitochondrial fragmentation in
509 monocytes treated with WATA-CM in comparison to control or BATA-CM treated monocytes. HFD is

510 known to induce mitochondrial fission in a number of cells that correlates with insulin resistance. A recent
511 report linked the two phenomena through *Drp1* action, as *Drp1* inhibition reversed HFD-induced insulin
512 resistance (Filippi et al., 2017). Furthermore, obese and diabetic humans have reduced *Mfn2* expression in
513 skeletal muscle. *Mfn2* positively correlates with insulin sensitivity (Bach et al., 2005), and *Mfn2* gene and
514 protein are significantly downregulated in liver cells of HFD-fed rats (Gan et al., 2013). In our analysis, the
515 expression of *Mfn2* negatively correlated with the abundance of Ly6C^{high} monocytes, while, the expression
516 of *Drp1* positively correlated with the BM abundance of Ly6C^{high} monocytes. Overall, our findings reveal
517 novel and distinct effects of adipocyte types on monocyte subset development that may occur through
518 changes in mitochondrial fitness.

519 Given that the proportion of Ly6C^{low} monocytes dropped in favour of a predominance of Ly6C^{high}
520 monocytes by 8 but not 3 weeks of HFD, it is possible that this subset change obeys a prior shift in their
521 metabolic orientation. Supporting these observations, exposure of monocytes to white adipocyte CM also
522 reduced their mitochondrial membrane potential. Furthermore, BMA-CM from 8-week HFD-fed mice also
523 lowered monocyte mitochondrial membrane potential compared to control BMA-CM and favoured
524 Ly6C^{high} predominance. Mechanistically, these data suggest that white adipocytes induce a monocyte
525 metabolic shift that may guide Ly6C^{high} monocyte prevalence.

526 In conclusion, we demonstrate an interconnectivity of cellular networks within the BM, a
527 vulnerability of the BM microenvironment to HFD, and a consequential myeloid lineage determination
528 likely due to BMA whitening. Given the vastly different metabolic and soluble factors between *bona fide*
529 white and brown adipocytes, it is easy to imagine that phenotypic changes in BMA can vastly alter the BM
530 microenvironment and the factors that surround hematopoietic cells. BMA whitening during HFD feeding
531 contributes to myelopoiesis and predominance of invasive Ly6C^{high} monocytes mediated by changes in
532 monocyte metabolism.

533 **Materials and Methods**

534 **Animal Procedures**

535 Mouse protocols were approved by the animal care committee (Protocol #20011850 to S.E.G. and
536 D.J.P., University of Toronto and #1000047074 to A.K., The Hospital for Sick Children). Three groups of
537 9-week-old male C57BL/6 mice were fed either low fat diet (10% kcal from fat; D12450Ji, Research Diets)
538 or HFD (60% kcal from fat; D12492i, Research Diets) for 3, 8, or 18 weeks. Each duration of feeding
539 involved at least 3 mice within each dietary group, and the precise number of mice evaluated in each
540 experiment is indicated in the figure legends. The feeding protocol was repeated with three independent
541 cohorts of mice, initiated at different times. The graphs illustrated include data collected from the three
542 cohorts. Logistically, not every mouse could be used for every type of experiment, and the number of mice
543 involved is indicated in each figure. Mice were singly caged to avoid stress and weight inequalities induced
544 by aggression of the dominant male to the subordinate male (Kappel et al., 2017). The cages were
545 maintained at 22°C on a 12h light/dark cycle, the diets were replaced once per week and various cage
546 enrichments were provided including switching the positioning of the cages throughout the study.

547 Body weight was measured twice per week. Upon completion of the respective feeding durations,
548 mice were fasted for 4 h, blood was drawn via tail vein and fasting blood glucose was measured with a
549 glucometer. Mice were euthanized by cervical dislocation. Tissues were dissected and flash frozen in liquid
550 nitrogen for RNA isolation. EWAT, blood and BM were immediately processed for flow cytometry
551 analysis.

552 **EWAT-Derived Stromal Vascular Fraction (SVF) Isolation**

553 EWAT-derived SVF was collected as previously described (Orr et al., 2013). Excised EWAT was
554 rinsed in PBS, minced and digested with 0.47wv/mL Liberase solution (Millipore Sigma, Cat No
555 5401054001) shaking at 200 rpm for 20 min at room temperature. SVF was isolated using a 70 µm cell
556 strainer, the enzymatic activity of Liberase was neutralized with DMEM containing HI-FBS for 5 min and

557 centrifuged at 500 ×g for 10 min. The supernatant containing adipocytes was removed, the pellet was re-
558 suspended in red blood cell lysis buffer for 5 min to remove erythrocytes and washed with PBS three times.

559 **BM Histology**

560 Extracted tibia and femur bones were fixed in 10% formalin for 48 h, decalcified in 14% EDTA
561 solution for 14 days, paraffin wax-embedded, and longitudinal sections were stained with H&E and Oil
562 Red O (Millipore Sigma; Cat No O0625) to visualize BM adiposity. Fifty imaging fields per mouse femur
563 were analyzed for the presence of adipocytes, assessed by blinded volunteers. Adipocyte area was
564 calculated using ImageJ software version 1.53.

565 **BM cell fractionation**

566 Following cervical dislocation, femurs and tibias were dissected from the mice fed control or the
567 HFD for 3, 8 or 18 weeks. Epiphyses were cut from one end of each bone, then bones were placed in 0.2
568 mL microtubes containing 18-gauge holes. Microtubes were placed inside 0.5 mL Eppendorf tubes
569 containing 100 µL media or PBS. This complex was centrifuged at 15,000 x g for 10 s to extract BM in the
570 pellet. BM supernatant was removed from the cellular pelleted fraction to be assessed by ELISA and used
571 for lactate quantification. BM cells were used for flow cytometry analysis, fluorescence-activated cell
572 sorting (FACS) to identify monocyte subsets and their gene expression, as well as for differentiation to
573 BM-derived monocytes.

574 **Primary Adipocyte Isolation and Culture to generate Conditioned Media**

575 Epididymal white and interscapular brown AT were dissected in sterile conditions, the tissues
576 underwent mechanical mincing and enzymatic digestion by collagenase type I (Worthington Biochemical
577 Corp, Cat No LS004197) at 4 mg/mL shaking for 1 hour. The digested adipocytes were then filtered through
578 a 200 µm cell strainer and centrifuged, washed twice and plated in adipocyte media: high glucose DMEM,
579 1% BSA, 0.5% FBS, and 1% Penicillin and Streptomycin for 24 h. BM adipocytes were isolated from the
580 floating fraction following BM isolation via centrifugation. The cells were counted and cultured in

581 adipocyte media overnight. Tissues from three mice were collected and the isolated cells were pooled in
582 each CM generating experiment.

583 ***In vitro*-generated BM-Derived Monocytes**

584 Murine primary BM cells were plated at 500,000 cells/mL on Thermo Scientific™ Nunc™ Non-
585 Treated 6-well plates (Cat No 1256680) with complete RPMI (Cat No 350-000-EL, Wisent BioProducts,
586 Saint-Jean-Baptiste, QC, Canada) and supplemented with recombinant mouse M-CSF (Peprotech Inc. Cat
587 No 315-02) at 20ng/mL for 5 days (Francke et al., 2011). Following 5 days of BM cell incubation on the
588 ultra-low attachment surface plates, the suspended cells have the signature of mature monocytes and can
589 be used for experimentation. These BM-derived differentiated monocytes were then collected, washed with
590 RMPI, centrifuged and re-suspended with various adipocyte CM for 18 h. Typically when BM cells were
591 collected three mice were independently processed at the same time. This process yielded three cohorts of
592 differentiated monocytes that would each be treated with Media-, WATA- and BATA-CM.

593 **Flow Cytometry**

594 Following red blood cell lysis, SVF, blood and the BM were washed with FACS buffer (PBS, 1%
595 (v/v) heat-inactivated FBS, 0.2% (w/v) BSA), stained with Aqua Live/Dead Antibody (ThermoFisher,
596 L34957) for 15 min in the dark, washed with FACS buffer again, blocked with anti-mouse CD16/32
597 antibody (eBioscience, 14-0161-86) for 15 min in the dark following a 30 min incubation with
598 corresponding antibody for each antigen **(**see **Table 1** for list of antibodies**).** The samples were then fixed,
599 read on LSR Fortessa cytometer (BD Biosciences) and data gated based on appropriate fluorescence minus
600 one (FMO) controls, and analyzed on the FlowJo software version 10 (Becton, Dickinson & Company).
601 See Figure S1 for gating strategies.

602 **Quantitative PCR (qPCR)**

603 RNA was extracted from cells or tissues using TRIzol™ (Life Technologies, Cat No 15596018),
604 then cDNA synthesized using the SuperScript VILO cDNA kit (Life Technologies, Cat No 11754250)

605 according to manufacturer's instructions. qPCR reactions were performed with predesigned TaqMan probes
606 (Life Technologies) on a StepOne Plus Real-Time PCR System (Applied Biosystems-ThermoFisher).
607 Duplicates of each cDNA sample were used for gene expression analysis and values were normalized to
608 the average of a set of the following housekeeping genes: Abt1, Hprt, and Eef2 by the $\Delta\Delta C_T$ method.

609 **BrdU incorporation**

610 The abcam protocol was followed to detect BrdU through an anti-BrdU antibody
611 (https://www.abcam.com/protocols/brdu-staining-protocol#BrdU%20labeling). BM-derived *in vitro*-
612 generated monocytes were labelled with 10 µM BrdU (ThermoFisher, 000103) during the 18-hour
613 treatment at 37C. The cells were then washed with FACS buffer, surface markers were stained as described
614 above and incubated in Foxp3 Fixation/Permeabilization Buffer (eBioscience, 00-5523-00) overnight. They
615 were then treated with 30 µg of DNAse I.9 (Sigma, 260913) for 1 hour, stained with anti-BrdU antibody
616 (abcam, ab6326) for 1 hour and then washed with FACS buffer in preparation to run on LSR Fortessa
617 Cytometer (BD Biosciences).

618 **Fluorescent Activated Cell Sorting of Monocytes**

619 BM from two femurs and tibias of 8-10-week-old chow-fed mice was used in the isolation of
620 monocyte subsets via fluorescent activated cell sorting using the FACS Aria Ilu instrument. $Gr1^-$ $CD115^+$
621 $CD11b^+$ and $Ly6C^+$ surface markers were used in identifying total monocytes and two subsets were
622 subsequently distinguished by the relative surface abundance (low and high) of Ly6C protein (Figure S1).
623 Isolated $Ly6C^{low}$ and $Ly6C^{high}$ monocytes were then validated for positive staining by antibodies CX3CR1
624 and CCR2 (Figure S1), respectively. Ly6C and Cd11b FMO controls shown in Figure S1B illustrated that
625 the gates drawn for $Ly6C^{low}$ and $Ly6C^{high}$ were confidently identifying cells positive for both these markers.

626 **Lactate quantification**

627 The BM content was fractioned into hematopoietic and supernatant portions by centrifugation at
628 1,600 rpm. The supernatant fraction was re-suspended in 500 µL of 1X PBS (supplemented with Protease

629 Cocktail Inhibitor, Sigma). One drop of the BM supernatant fraction was placed on the Blood Lactate Meter
630 Lactate Plus (Nova Biomedical) for the quantification of its lactate content. The values were normalized to
631 the undiluted BM isolated from the femur.

632 **Cell Metabolism Analysis**

633 Oxygen consumption (OCR) and extracellular acidification rates were measured using a Seahorse
634 XFe96 analyzer (Seahorse Bioscience). Seahorse 96-well cell culture plates were pretreated with 1 μg/cm^2
635 Corning™ Cell-Tak Cell and Tissue Adhesive (Fisher Scientific, Cat No CB40240) and FACS sorted
636 Ly6C^{low} or Ly6C^{high} monocytes were seeded at 100,000 cells/well, allowed to equilibrate for 1 h in XF base
637 medium supplemented with 11 mM glucose, 1 mM sodium pyruvate and 2 mM Glutamine. Following
638 baseline measurements, FCCP was injected at 1 mM and thereafter an injection of Antimycin A/ Rotenone.
639 Cells were counted following the seahorse assay to test for changes in cellular detachment between the
640 conditions.

641 **Immunofluorescence Staining for Super-Resolution Microscopy**

642 Monocytes were spun down onto coverslips and fixed with 4% paraformaldehyde for 15 min.
643 Thereafter, the cells were rinsed with PBS and permeabilized with 0.1% Triton X-100 for 10 min. The cells
644 were then blocked with 2% BSA in PBS at 4℃ overnight. The cells were then incubated with the primary
645 antibody, Tom20 (FL-145, Santa Cruz, sc-11415), in a 1:100 dilution in blocking buffer at 4℃ overnight.
646 Thereafter, the cells were incubated with Alexa Fluor 488 anti-rabbit secondary antibody (1:100) for 2 h at
647 room temperature. Cells were incubated with Alexa Fluor 568 Phalloidin (1:100) for 3 h at room
648 temperature. Coverslips were then mounted by ProLong Diamond (Thermo Fisher Scientific) and allowed
649 to dry for two days. The images were acquired via Zeiss LSM880 Airyscan super resolution microscopy
650 and the images were processed via Fiji software. The percentage of monocytes displaying each
651 mitochondrial morphology (fragmented, intermediate, or tubulated) was scored as described previously
652 (Rambold et al., 2011).
653

654 **Colony-Forming Unit Assay**

655 *In vitro* differentiated BM-derived monocytes (5×10^5 cell/ml) were treated as indicated, then
656 pelleted and suspended in Iscove's modified Dulbecco's medium to 2×10^5 cell/ml, diluted in MethoCult
657 GF-M3434 medium and plated at 20,000 cells/35 mm well in a 6-well plate of low-adherence culture-ware
658 (STEMCELL Technologies, Inc.), in triplicate. The colonies that grew had distinct cell lineages and
659 morphologies as defined in detail by the STEMCELL manual for MethoCult GF-M3434 methylcellulose
660 media. After 7-10 days, colonies were counted, using an inverted light microscope, and identified as: Burst-
661 forming unit-erythroid (BFU-E), Colony-forming unit-granulocyte, erythrocyte, macrophage,
662 megakaryocyte (CFU-GEMM), CFU-granulocyte (CFU-G) or CFU-macrophage (CFU-M), based on the
663 STEMCELL Technologies detailed instructions. Of note, CFU-GEMM progenitors are also known as
664 CMP, and GMP progenitors give rise to the CFU-G and CFU-M lineages (immediate precursors of
665 monoblasts and monocytes) that form colonies in this assay (https://www.stemcell.com/hematopoietic-
666 stem-and-progenitor-cells-lp.html).

667 **ELISA Determinations**

668 The BM content was fractioned into hematopoietic and supernatant portions by centrifugation at
669 1,600 rpm. The supernatant fraction was re-suspended in 500ul of 1X PBS (supplemented with Protease
670 Cocktail Inhibitor, Sigma). Total protein content was estimated by Pierce™ BCA Protein Assay Kit
671 (ThermoFisher Scientific). Subsequently, mouse TNF, IL-1b, IL-6, CXCL1 and CCL2 ELISAs were
672 carried out according to the manufacturers' instructions. All Mouse DuoSet ELISA kits were purchased
673 from R&D systems. The individual protein contents were finally normalised to total protein content.

674 **Statistical Analysis**

675 Data are expressed as means ± SEM. An unpaired Student's T test was used to detect differences
676 in data sets with one variable such as that in Figure S2. A one-way ANOVA with Tukey post-test was used
677 to detect differences in data sets of two or more variables. Statistical significance was set at $P < 0.05$. Data

678 analysis and statistics tests were done using GraphPad Prism version 6 (GraphPad Software), Flow Jo
679 Software version 10.4 and figures were prepared using Adobe Illustrator CS6 version 16.0.
680 Correlative analysis statistics were conducted using the linear regression analysis via GraphPad
681 Prism version 6 (GraphPad Software) testing whether slopes and intercepts are significantly different. The
682 r^2 represents the goodness of the fit while the P values greater than 0.05 represent whether the slope of the
683 line of best fit is significantly non-zero.
684

Acknowledgements

We thank Dr. Spencer Freeman for helpful discussion. This work was supported by Canadian Institutes of Health Research (CIHR) Foundation Grant (FND-143203 to A.K. and FDN-14333 to D.J.P. Studentship support for P.B. was from a Banting & Best Diabetes Centre-Novo Nordisk Graduate Studentship (2017-2019) and a SickKids Research Training Centre Award (2019- 2020).

Author Contribution

P.B., A.K. and S.E.G. conceived the study design. P.B. coordinated and performed experiments and analyzed the data. M.W., J.S., I.T., N.S., L.Z., Z.L., A.L., T.M., Y.Z. and T.S. participated in experimental work and data collection. P.J.B. contributed with valuable advice, troubleshooting, and performed and analyzed experiments. A.K., D.J.P., S.E.G. and C.R. provided access to resources and facilities. P.B. and A.K. wrote the manuscript, and all authors read and approved it.

697 **References:**

698 Adler, B.J., Kaushansky, K., and Rubin, C.T. (2014). Obesity-driven disruption of
699 haematopoiesis and the bone marrow niche. Nat. Rev. Endocrinol. *10*, 737–748.

700 Ambrosi, T.H., Scialdone, A., Graja, A., Gohlke, S., Jank, A.M., Bocian, C., Woelk, L., Fan, H.,
701 Logan, D.W., Schürmann, A., et al. (2017). Adipocyte Accumulation in the Bone Marrow during
702 Obesity and Aging Impairs Stem Cell-Based Hematopoietic and Bone Regeneration. Cell Stem
703 Cell *20*, 771–784.e6.

704 Auffray, C., Fogg, D., Garfa, M., Gaelle, E., Join-Lambert, O., Kayal, S., Sarnacki, S., Ana, C.,
705 Lauvau, G., and Geissmann, F. (2007). Monitoring of Blood Vessels and Tissues by a Population
706 of Monocytes with Patrolling Behavior. *317*, 666–671.

707 Auffray, C., Fogg, D.K., Narni-Mancinelli, E., Senechal, B., Trouillet, C., Saederup, N.,
708 Leemput, J., Bigot, K., Campisi, L., Abitbol, M., et al. (2009). CX 3 CR1 + CD115 + CD135 +
709 common macrophage/DC precursors and the role of CX 3 CR1 in their response to inflammation
710 . J. Exp. Med. *206*, 595–606.

711 Bach, D., Naon, D., Pich, S., Soriano, F.X., Vega, N., Rieusset, J., Laville, M., Guillet, C.,
712 Boirie, Y., Wallberg-henriksson, H., et al. (2005). Expression of Mfn2, the Charcot-Marie-Tooth
713 Neuropathy Type 2A Gene, in Human Skeletal Muscle. Diabetes *54*, 2685–2693.

714 Bagchi, M., Kim, L.A., Boucher, J., Walshe, T.E., Kahn, C.R., and Amore, P.A.D. (2013).
715 Vascular endothelial growth factor is important for brown adipose tissue development and
716 maintenance. FASEB J. *27*, 3257–3271.

717 Beattie, L., Sawtell, A., Mann, J., Frame, T.C.M., Teal, B., de Labastida Rivera, F., Brown, N.,
718 Walwyn-Brown, K., Moore, J.W.J., MacDonald, S., et al. (2016). Bone marrow-derived and
719 resident liver macrophages display unique transcriptomic signatures but similar biological
720 functions. J. Hepatol. *65*, 758–768.

721 Boniakowski, A.E., Kimball, A.S., Joshi, A., Schaller, M., Davis, F.M., denDekker, A., Obi,
722 A.T., Moore, B.B., Kunkel, S.L., and Gallagher, K.A. (2018). Murine macrophage chemokine
723 receptor CCR2 plays a crucial role in macrophage recruitment and regulated inflammation in
724 wound healing. Eur. J. Immunol. *48*, 1445–1455.

725 Boroumand, P., and Klip, A. (2020). Bone marrow adipose cells – cellular interactions and
726 changes with obesity. J. Cell Sci. *1*, 1–8.

727 Bowers E., Singer K. (2021) Obesity-induced inflammation: The impact of the hematopoietic
728 stem cell niche. JCI Insight. *6*, e145295.

729 Buck, M.D., Sowell, R.T., Kaech, S.M., and Pearce, E.L. (2017). Metabolic Instruction of
730 Immunity. Cell *169*, 570–586.

731 Cassado, A.A., D'Império Lima, M.R., and Bortoluci, K.R. (2015). Revisiting mouse peritoneal
732 macrophages: Heterogeneity, development, and function. Front. Immunol. *6*, 1–9.

733 Castoldi, A., De Souza, C.N., Saraiva Câmara, N.O., and Moraes-Vieira, P.M. (2016). The
734 macrophage switch in obesity development. Front. Immunol. *6*, 1–11.

735 Centers for Disease Control and Prevention, C. (2017). National Diabetes Statistics Report:
736 Estimates of Diabetes and Its Burden in the United States. Atlanta, GA: Centers for Disease
737 Control and Prevention; 2017. US Dep. Heal. Hum. Serv.

738 Challen, G.A., Boles, N., Lin, K.K.Y., and Goodell, M.A. (2009). Mouse hematopoietic stem
739 cell identification and analysis. Cytom. Part A *75*, 14–24.

740 Cuminetti, V., and Arranz, L. (2019). Bone Marrow Adipocytes: The Enigmatic Components of
741 the Hematopoietic Stem Cell Niche. J. Clin. Med. *8*, 707.

742 Doucette, C.R., Horowitz, M.C., Berry, R., MacDougald, O.A., Anunciado-Koza, R., Koza,
743 R.A., and Rosen, C.J. (2015a). A High Fat Diet Increases Bone Marrow Adipose Tissue (MAT)
744 But Does Not Alter Trabecular or Cortical Bone Mass in C57BL/6J Mice. J Cell Physiol *230*,
745 2032–2037.

746 Doucette, C.R., Horowitz, M.C., Berry, R., Macdougald, O.A., Anunciado-Koza, R., Koza, R.A.,
747 and Rosen, C.J. (2015b). A High Fat Diet Increases Bone Marrow Adipose Tissue (MAT) But
748 Does Not Alter Trabecular or Cortical Bone Mass in C57BL/6J Mice. J. Cell. Physiol. *230*,
749 2032–2037.

750 Elias, I., Franckhauser, S., Ferré, T., Vilà, L., Tafuro, S., Muñoz, S., Roca, C., Ramos, D., Pujol,
751 A., Riu, E., et al. (2012). Adipose Tissue Overexpression of Vascular Endothelial Growth Factor
752 Protects Against Diet-Induced Obesity and Insulin Resistance. Diabetes *61*, 1801–1813.

753 Filippi, B.M., Abraham, M.A., Silva, P.N., Bauer, P. V, Rocheleau, J. V, Lam, T.K.T., Filippi,
754 B.M., Abraham, M.A., Silva, P.N., Rasti, M., et al. (2017). Mitochondrial Fission Changes in the
755 Dorsal Vagal Report Dynamin-Related Protein 1-Dependent Mitochondrial Fission Changes in
756 the Dorsal Vagal Complex Regulate Insulin Action. CellReports *18*, 2301–2309.

757 Fink, L.N., Costford, S.R., Lee, Y.S., Jensen, T.E., Bilan, P.J., Oberbach, A., Blüher, M.,
758 Olefsky, J.M., Sams, A., and Klip, A. (2014a). Pro-Inflammatory macrophages increase in
759 skeletal muscle of high fat-Fed mice and correlate with metabolic risk markers in humans.
760 Obesity *22*, 747–757.

761 Fink, L.N., Costford, S.R., Lee, Y.S., Jensen, T.E., Bilan, P.J., Oberbach, A., Blüher, M.,
762 Olefsky, J.M., Sams, A., and Klip, A. (2014b). Pro-Inflammatory macrophages increase in
763 skeletal muscle of high fat-Fed mice and correlate with metabolic risk markers in humans.
764 Obesity *22*, 747–757.

765 Francke, A., Herold, J., Weinert, S., Strasser, R.H., and Braun-Dullaeus, R.C. (2011). Generation
766 of mature murine monocytes from heterogeneous bone marrow and description of their
767 properties. J. Histochem. Cytochem. *59*, 813–825.

768 Friedrich, K., Sommer, M., Strobel, S., Thrum, S., and Blüher, M. (2019). Perturbation of the
769 Monocyte Compartment in Human Obesity. Front. Immunol. *10*, 1–10.

770 Gan, K., Wang, C., Chen, J., Zhu, C., and Song, G. (2013). Mitofusin-2 ameliorates high-fat diet-
771 induced insulin resistance in liver of rats. *19*, 1572–1581.

772 Garvey, W.T., Henry, R.R., Kern, P.A., Saghizadeh, M., and Ong, J.M. (2008). The expression

773 of TNF alpha by human muscle. Relationship to insulin resistance. J. Clin. Invest. *97*, 1111–
774 1116.

775 Geissmann, F., Jung, S., and Littman, D.R. (2003). Blood monocytes consist of two principal
776 subsets with distinct migratory properties. Immunity *19*, 71–82.

777 Gibbings, S.L., Goyal, R., Desch, A.N., Leach, S.M., Prabagar, M., Atif, S.M., Bratton, D.L.,
778 Janssen, W., and Jakubzick, C. V. (2015). Transcriptome analysis highlights the conserved
779 difference between embryonic and postnatal-derived alveolar macrophages. Blood *126*, 1357–
780 1366.

781 Gottlieb, R.A., and Bernstein, D. (2017). Mitochondrial Remodeling: Rearranging, Recycling,
782 and Reprogramming. Cell Calcium *60*, 88–101.

783 Griffin, C., Eter, L., Lanzetta, N., Abrishami, S., Varghese, M., McKernan, K., Muir, L., Lane,
784 J., Lumeng, C.N.-K., and Singer, K. (2018). TLR4, TRIF, and MyD88 are essential for
785 myelopoiesis and CD11c+ adipose tissue macrophage production in obese mice. J. Biol. Chem.
786 jbc.RA117.001526.

787 Hamann, A. (2017). Obesity Update 2017. Diabetologe.

788 Kamei, N., Tobe, K., Suzuki, R., Ohsugi, M., Watanabe, T., Kubota, N., Ohtsuka-kowatari, N.,
789 Kumagai, K., Sakamoto, K., Kobayashi, M., et al. (2006). Overexpression of Monocyte
790 Chemoattractant Protein-1 in Adipose Tissues Causes Macrophage Recruitment and Insulin
791 Resistance *. J. Biol. Chem. *281*, 26602–26614.

792 Kappel, S., Hawkins, P., and Mendl, M. (2017). To Group or Not to Grou? Good Practice for
793 Housing Male Laboratory Mice. Animals 1–25.

794 Kelly, B., and O'Neill, L.A. (2015). Metabolic reprogramming in macrophages and dendritic
795 cells in innate immunity. Cell Res. *25*, 771–784.

796 Kohyama, M., Matsuoka, S., Shida, K., Sugihara, F., Aoshi, T., Kishida, K., Ishii, K.J., and
797 Arase, H. (2016). Monocyte infiltration into obese and fibrilized tissues is regulated by PILRα.
798 Eur. J. Immunol. *46*, 1214–1223.

799 Kratofil, R.M., Kubes, P., and Deniset, J.F. (2017). Monocyte conversion during inflammation
800 and injury. Arterioscler. Thromb. Vasc. Biol. *37*, 35–42.

801 Krings, A., Rahman, S., Huang, S., Lu, Y., Czernik, P.J., and Lecka-Czernik, B. (2012). Bone
802 marrow fat has brown adipose tissue characteristics, which are attenuated with aging and
803 diabetes. Bone *50*, 546–552.

804 Lanthier, N., Molendi-Coste, O., Horsmans, Y., van Rooijen, N., Cani, P.D., and Leclercq, I.A.
805 (2010). Kupffer cell activation is a causal factor for hepatic insulin resistance. Am. J. Physiol.
806 Liver Physiol. *298*, G107–G116.

807 Lee, M.K.S., and Murphy, A.J. (2019). Glycolysis Is Required for LPS-Induced Activation and
808 Monocytes. *10*, 1–10.

809 Lessard, A.J., LeBel, M., Egarnes, B., Préfontaine, P., Thériault, P., Droit, A., Brunet, A., Rivest,

810 S., and Gosselin, J. (2017). Triggering of NOD2 Receptor Converts Inflammatory Ly6Chighinto
811 Ly6ClowMonocytes with Patrolling Properties. Cell Rep. *20*, 1830–1843.

812 Leung, D.W., Cachianes, G., Kuang, W., Goeddel, D. V, and Ferrara, N. (1989). Vascular
813 Endothelial Growl th Factor Is a Secreted Angiogenic Mitogen. Science (80-.). *246*, 1306–9.

814 Lin, S.L., Castano, A.P., Nowlin, B.T., Lupher, M.L., and Duffield, J.S. (2009). Bone Marrow
815 Ly6Chigh Monocytes Are Selectively Recruited to Injured Kidney and Differentiate into
816 Functionally Distinct Populations. J. Immunol. *183*, 6733–6743.

817 Liu, T., Sun, Y.-C., Cheng, P., and Shao, H.-G. (2019). Adipose tissue macrophage-derived
818 exosomal miR-29a regulates obesity-associated insulin resistance. Biochem. Biophys. Res.
819 Commun.

820 Lumeng, C.N., Deyoung, S.M., Bodzin, J.L., and Saltiel, A.R. (2007). Increased Inflammatory
821 Properties of Adipose Tissue Macrophages Recruited During Diet-Induced Obesity. Diabetes *56*,
822 16–23.

823 Lumeng, C.N., Delproposto, J.B., Westcott, D.J., and Saltiel, A.R. (2008). Phenotypic Switching
824 of Adipose Tissue Macrophages With Obesity Is Generated by Spatiotemporal Differences in
825 Macrophage Subtypes. Diabetes *57*, 3239–3246.

826 Manicone, A.M., Gong, K., Johnston, L.K., and Giannandrea, M. (2016). Diet-induced obesity
827 alters myeloid cell populations in naïve and injured lung. Respir. Res. *17*, 24.

828 Nagareddy, P.R., Kraakman, M., Masters, S.L., Stirzaker, R.A., Gorman, D.J., Grant, R.W.,
829 Dragoljevic, D., Hong, E.S., Abdel-Latif, A., Smyth, S.S., et al. (2014). Adipose tissue
830 macrophages promote myelopoiesis and monocytosis in obesity. Cell Metab. *19*, 821–835.

831 Nakagami, H. (2013). The Mechanism of White and Brown Adipocyte Differentiation. Diabetes
832 Metab. J. *37*, 85–90.

833 Nascimento, E.B.M., Boon, M.R., and van Marken Lichtenbelt, W.D. (2014). Fat cells gain new
834 identities. Sci. Transl. Med. *6*, 1–4.

835 Nov, O., Shapiro, H., Ovadia, H., Tarnovscki, T., Dvir, I., Shemesh, E., Kovsan, J., Shelef, I.,
836 Carmi, Y., Voronov, E., et al. (2013). Interleukin-1β Regulates Fat-Liver Crosstalk in Obesity by
837 Auto-Paracrine Modulation of Adipose Tissue Inflammation and Expandability. PLoS One *8*.

838 O'Neill, L., Kishton, R., and Rathmell, J. (2016). A guide to immunometabolism for
839 immunologists. Nat. Rev. Immunol. *16*, 553–565.

840 Orr, J.S., Kennedy, A.J., and Hasty, A.H. (2013). Isolation of Adipose Tissue Immune Cells. J.
841 Vis. Exp. 1–7.

842 Patel, A.A., Zhang, Y., Fullerton, J.N., Boelen, L., Rongvaux, A., Maini, A.A., Bigley, V.,
843 Flavell, R.A., Gilroy, D.W., Asquith, B., et al. (2017). The fate and lifespan of human monocyte
844 subsets in steady state and systemic inflammation. J. Exp. Med. *214*, 1913–1923.

845 Pence, B.D., and Yarbro, J.R. (2019). Classical monocytes maintain ex vivo glycolytic
846 metabolism and early but not later inflammatory responses in older adults. Immun. Ageing *16*,

1–8.

Pham, T.T., Ivaska, K.K., Hannukainen, J.C., Virtanen, K.A., Lidell, M.E., Parkkola, R., Piirola, S., Oikonen, V., Nuutila, P., Biology, C., et al. (2020). Human bone marrow adipose tissue is a metabolically active and insulin sensitive distinct fat depot. J. Clin. Endocrinol. Metab. *pii*, dgaa216.

Rambold A.S., Kostelecky B., Elia N., Lippincott-Schwartz J. (2011) Tubular network formation protects mitochondria from autophagosomal degradation during nutrient starvation. Proc Natl Acad Sci U S A. *108*, 10190-10195.

Renovato-Martins, M., Matheus, M.E., de Andrade, I.R., Moraes, J.A., da Silva, S.V., Citelli dos Reis, M., de Souza, A.A.P., da Silva, C.C., Bouskela, E., and Barja-Fidalgo, C. (2017). Microparticles derived from obese adipose tissue elicit a pro-inflammatory phenotype of CD16 + , CCR5 + and TLR8 + monocytes. Biochim. Biophys. Acta - Mol. Basis Dis. *1863*, 139–151.

Rosen, E.D., and MacDougald, O.A. (2006). Adipocyte differentiation from the inside out. Nat. Rev. Mol. Cell Biol. *7*, 885–896.

Scheller, E.L., Doucette, C.R., Learman, B.S., Cawthorn, W.P., Khandaker, S., Schell, B., Wu, B., Ding, S.Y., Bredella, M.A., Fazeli, P.K., et al. (2015). Region-specific variation in the properties of skeletal adipocytes reveals regulated and constitutive marrow adipose tissues. Nat. Commun. *6*, 1–13.

Scheller, E.L., Khoury, B., Moller, K.L., Wee, N.K.Y., Khandaker, S., Kozloff, K.M., Abrishami, S.H., Zamarron, B.F., and Singer, K. (2016). Changes in skeletal integrity and marrow adiposity during high-fat diet and after weight loss. Front. Endocrinol. (Lausanne). *7*, 1–13.

Shanmugam, N., Reddy, M.A., Guha, M., and Natarajan, R. (2003). High glucose-induced expression of proinflammatory cytokine and chemokine genes in monocytic cells. Diabetes *52*, 1256–1264.

Sharma, M., Boytard, L., Hadi, T., Koelwyn, G., Simon, R., Ouimet, M., Seifert, L., Spiro, W., Yan, B., Hutchison, S., et al. (2020). Enhanced glycolysis and HIF-1 α activation in adipose tissue macrophages sustains local and systemic interleukin-1 β production in obesity. Sci. Rep. *10*, 1–12.

Silva, S. V., Renovato-martins, M., Ribeiro-pereira, C., Citelli, M., and Barja-fidalgo, C. (2016). Obesity Modifies Bone Marrow Microenvironment and Directs Bone Marrow Mesenchymal Cells to Adipogenesis. Obes. Biol. Integr. Physiol. *24*, 2522–2532.

Singer, K., DelProposto, J., Lee Morris, D., Zamarron, B., Mergian, T., Maley, N., Cho, K.W., Geletka, L., Subbaiah, P., Muir, L., et al. (2014). Diet-induced obesity promotes myelopoiesis in hematopoietic stem cells. Mol. Metab. *3*, 664–675.

Singer K., Maley N., Mergian T., DelProposto J., Cho K.W., Zamarron B.F., Martinez-Santibanez G., Geletka L., Muir L., Wachowiak P., et al. (2015). Differences in Hematopoietic Stem Cells Contribute to Sexually Dimorphic Inflammatory Responses to High Fat Diet-induced Obesity. J Biol Chem. *290*, 13250-13262.

886 De Souza, C.T., Araujo, E.P., Bordin, S., Ashimine, R., Zollner, R.L., Boschero, A.C., Saad,
887 M.J.A., and Velloso, L.A. (2005). Consumption of a fat-rich diet activates a proinflammatory
888 response and induces insulin resistance in the hypothalamus. Endocrinology *146*, 4192–4199.

889 Sulston, R.J., and Cawthorn, W.P. (2016). Bone marrow adipose tissue as an endocrine organ:
890 close to the bone? Horm. Mol. Biol. Clin. Investig. *28*, 21–38.

891 Takahashi, K., Mizuarai, S., Araki, H., Mashiko, S., Ishihara, A., Kanatani, A., Itadani, H., and
892 Kotani, H. (2003). Adiposity Elevates Plasma MCP-1 Levels Leading to the Increased CD11b-
893 positive Monocytes in Mice *. J. Biol. Chem. *278*, 46654–46660.

894 Thapa, B., and Lee, K. (2019). Metabolic influence on macrophage polarization and
895 pathogenesis. BMB Rep. *52*, 360–372.

896 Tratwal, J., Labella, R., Bravenboer, N., and Kerckhofs, G. (2020). Reporting Guidelines ,
897 Review of Methodological Standards , and Challenges Toward Harmonization in Bone Marrow
898 Adiposity Research . Report of the Methodologies Working Group of the International Bone
899 Marrow Adiposity Society. Front. Endocrinol. (Lausanne). *11*, 1–36.

900 Ussar, S., Lee, K., Dankel, S., Boucher, J., Haering, M., Kleinridders, A., Thomou, T., Xue, R.,
901 Macoteia, Y., Cypess, A., et al. (2014). Asc-1, PAT2 and P2RX5 are novel cell surface markers
902 for white, beige and brown adipocytes. Sci Transl Med *247*, 247ra103.
903 doi:10.1126/scitranslmed.3008490. Asc-1,.

904 Verdeguer, F., and Aouadi, M. (2017). Macrophage heterogeneity and energy metabolism. Exp.
905 Cell Res. *360*, 35–40.

906 Weisberg, S.P., McCann, D., Desai, M., Rosenbaum, M., Leibel, R.L., and Ferrante, A.W.
907 (2003). Obesity is associated with macrophage accumulation in adipose tissue. J. Clin. Invest.
908 *112*, 1796–1808.

909 Weisberg, S.P., Hunter, D., Huber, R., Lemieux, J., Slaymaker, S., Vaddi, K., Charo, I., Leibel,
910 R.L., and Ferrante Jr, A.W. (2006). CCR2 modulates inflammatory and metabolic effects of
911 high-fat feeding. J. Clin. Invest. *116*, 115–124.

912 WHO (2016). World Health Organization. Global Report on Diabetes. Geneva, Switzerland.

913 Yao C.H., Wang R., Wang Y., Kung C.P., Weber J.D., Patti G.J. (2019) Mitochondrial fusion
914 supports increased oxidative phosphorylation during cell proliferation. Elife. *8*, e41351.

915 Yáñez A., Coetzee S.G., Olsson A., Muench D.E., Berman B.P., Hazelett D.J., Salomonis N.,
916 Grimes H.L., Goodridge H.S. (2017) Granulocyte-Monocyte Progenitors and Monocyte-
917 Dendritic Cell Progenitors Independently Produce Functionally Distinct Monocytes. Immunity.
918 *47*, 890-902.

919

Figure 1

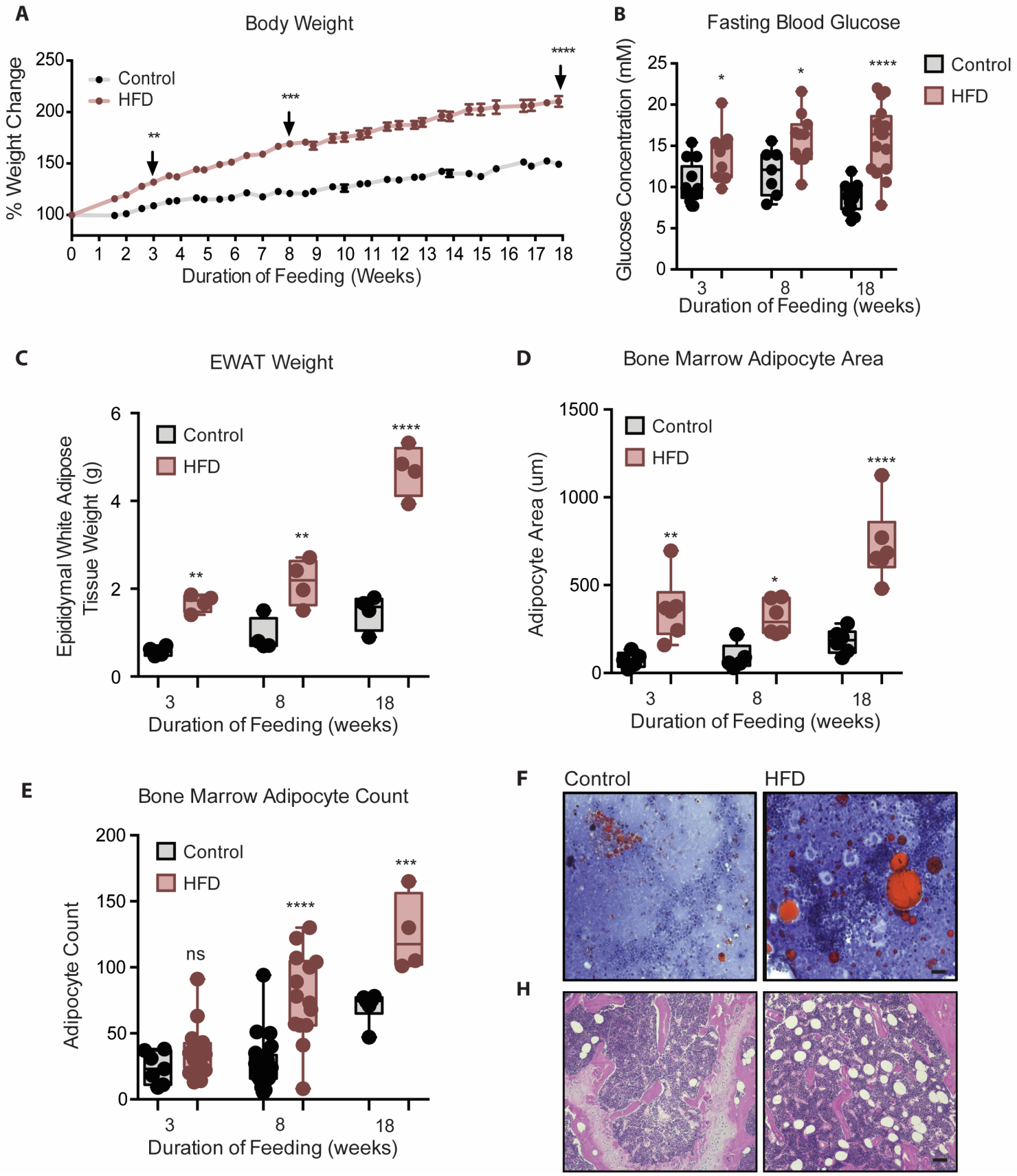
A
Body Weight
% Weight Change
Control
HFD
**
***
****
Duration of Feeding (Weeks)
B
Fasting Blood Glucose
Glucose Concentration (mM)
Control
HFD
Duration of Feeding (weeks)
C
EWAT Weight
Epididymal White Adipose Tissue Weight (g)
Control
HFD
Duration of Feeding (weeks)
D
Bone Marrow Adipocyte Area
Adipocyte Area (um)
Control
HFD
Duration of Feeding (weeks)
E
Bone Marrow Adipocyte Count
Adipocyte Count
Control
HFD
ns
Duration of Feeding (weeks)
F
Control
HFD
H

920 **Figure 1. Mice fed HFD increased body weight, fasting blood glucose, visceral and bone marrow**
921 **adipose tissue.** [A] Body weight was measured twice a week throughout the course of feeding. (n=14 per
922 dietary group). [B] Mice were fasted for 4 h after which fasting blood glucose was measured. (n=9-14 per
923 dietary group). [C] EWAT was weighed the day of sacrifice. (n=4 per dietary group at each feeding
924 duration). [D] Area covered by BM adipocytes were measured following H&E to visualize adipocyte
925 ghosts using quantified using ImageJ software. (n=6 mice in each dietary group at each feeding duration).
926 [E] BM adipocyte numbers per field were blindly counted following H&E staining using ImageJ software
927 version 1.53 (n=4-14 mice in each dietary group per feeding duration). [F] Representative images of
928 femurs from mice fed control and HFD diet for 3 weeks, that were fixed in formalin for 2 days followed
929 by 14 days EDTA decalcification and subsequently stained with Oil Red O (ORO). [G] Representative
930 images of femurs from mice fed control and HFD diet for 8 weeks, that were fixed in formalin for 2 days
931 followed by 14 days EDTA decalcification and subsequently stained with H&E. Scale bar is 25μm.
932 Results are expressed as mean ± SEM, n=4-14 mice per group. One-way ANOVA was used for statistical
933 analysis at each dietary group and across feeding periods. *P < 0.05, **P < 0.01, ***P < 0.001, ****P <
934 0.0001 and ns = not significant P > 0.05.
935
936

Figure 2

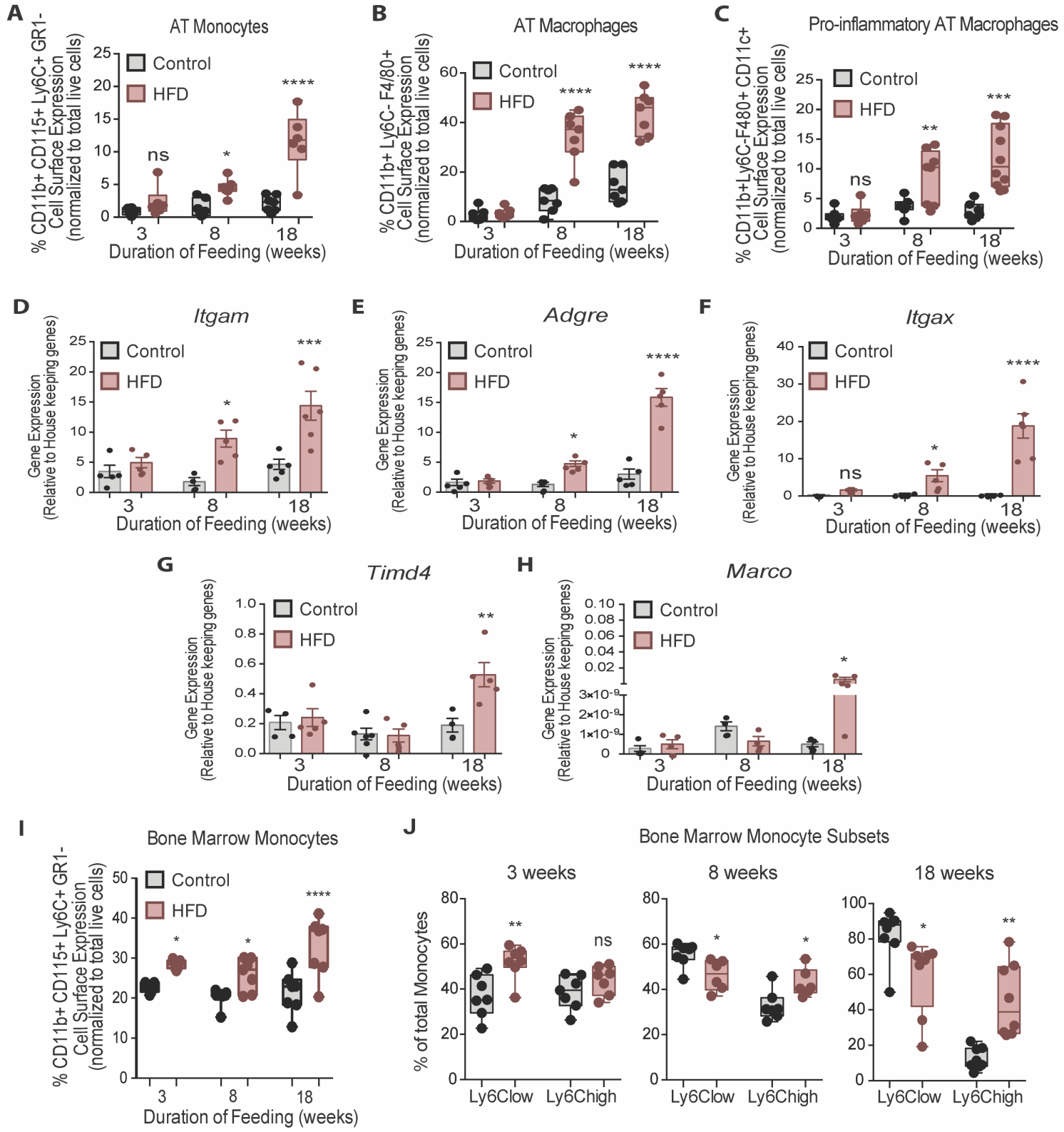
A
AT Monocytes
% CD11b+ CD115+ Ly6C+ GR1- Cell Surface Expression (normalized to total live cells)
Control
HFD
ns
*
****
Duration of Feeding (weeks)
B
AT Macrophages
% CD11b+ Ly6C- F4/80+ Cell Surface Expression (normalized to total live cells)
C
Pro-inflammatory AT Macrophages
% CD11b+Ly6C-F480+ CD11c+ Cell Surface Expression (normalized to total live cells)
D
Itgam
Gene Expression (Relative to House keeping genes)
E
Adgre
F
Itgax
G
Timd4
H
Marco
I
Bone Marrow Monocytes
J
Bone Marrow Monocyte Subsets
3 weeks
8 weeks
18 weeks
% of total Monocytes
Ly6Clow
Ly6Chigh

937 **Figure 2. Bone marrow monocytes increased prior to adipose tissue macrophages.** Analysis of
938 monocytes and macrophages in the stromal vascular fraction (SVF) of adipose tissue via flow cytometry
939 analysis, identified first by size and granularity through forward and side scatter and then using the
940 following markers: CD11b CD115 F4/80 Ly6C GR1 CD11c. (n=7-10 mice in each dietary group at each
941 feeding duration): [A] monocytes, [B] total macrophages, [C] pro-inflammatory macrophages. [D-F] Whole
942 adipose tissue gene expression of the myeloid marker *Itgam,* macrophage marker *Adgre* and pro-
943 inflammatory myeloid marker *Itgax* by RTqPCR. Each symbol represents a biological replicate analyzed
944 in duplicate and normalized to average of a group of housekeeping genes. (n=5 mice in each dietary group
945 at each feeding duration). [G-H] Gene expression analysis of embryonic derived tissue resident macrophage
946 markers *Timd4* and *Marco* by RTqPCR. Each symbol represents a biological replicate analyzed in duplicate
947 and normalized to average of a group of housekeeping genes. (n=3-5 mice in each dietary group at each
948 feeding duration). [I] Flow cytometry analysis of total BM monocytes (n=7 mice in each dietary group at
949 each feeding duration). [J] Monocyte subsets in the bone marrow with HFD-feeding (n=7 mice in each
950 dietary group at each feeding duration). Results are expressed as mean ± SEM. One-way ANOVA was used
951 for statistical analysis at each dietary group and across feeding periods. *$P < 0.05$, **$P < 0.01$, ***$P <$
952 0.001, ****$P < 0.0001$ and ns = not significant $P > 0.05$.

953

Figure 3

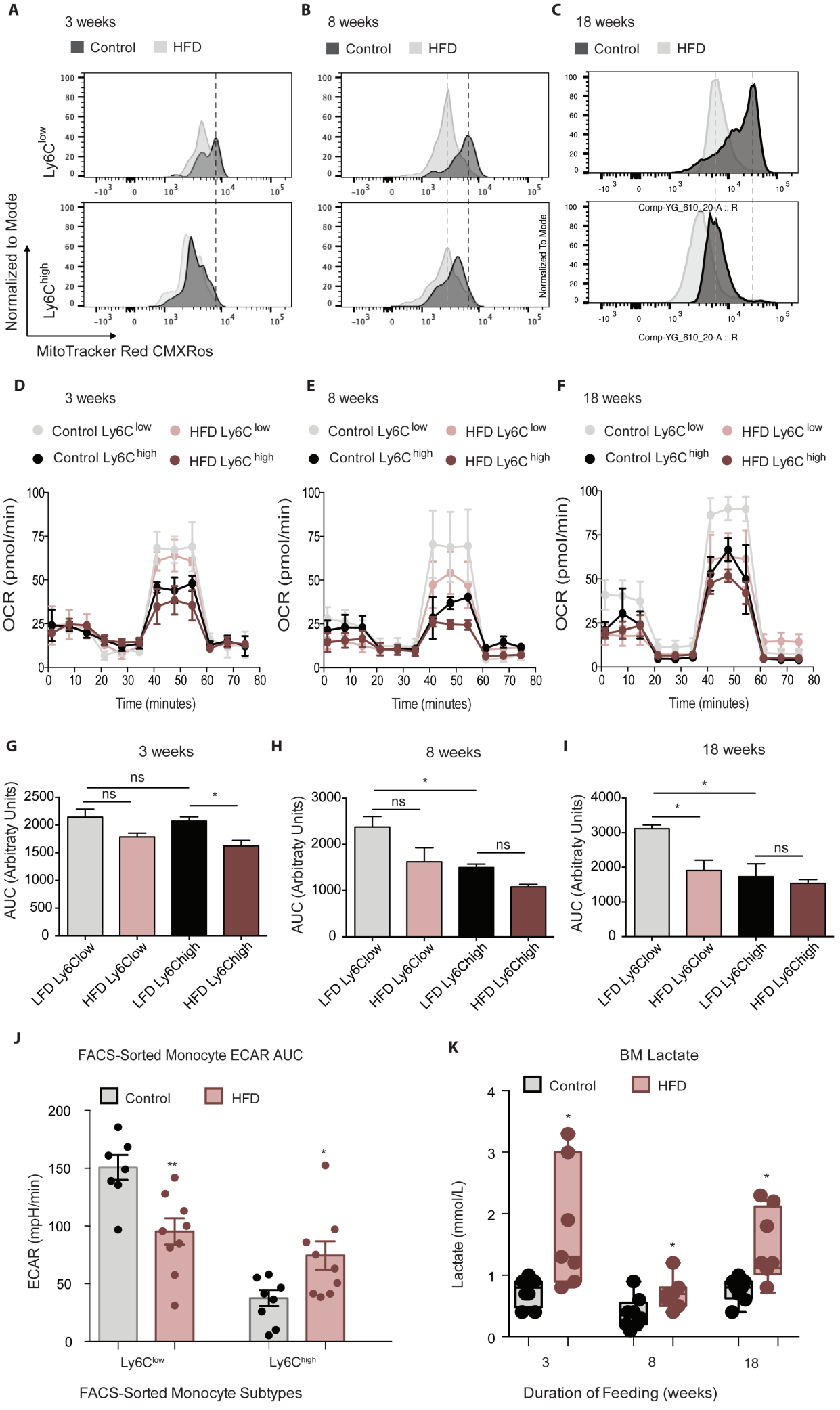
A
3 weeks
Control
HFD
B
8 weeks
C
18 weeks
Ly6C low
Ly6C high
Normalized to Mode
MitoTracker Red CMXRos
Comp-YG_610_20-A :: R
D
E
F
Control Ly6C low
HFD Ly6C low
Control Ly6C high
HFD Ly6C high
OCR (pmol/min)
Time (minutes)
G
H
I
AUC (Arbitraty Units)
ns
*
LFD Ly6Clow
HFD Ly6Clow
LFD Ly6Chigh
HFD Ly6Chigh
J
FACS-Sorted Monocyte ECAR AUC
ECAR (mpH/min)
**
FACS-Sorted Monocyte Subtypes
K
BM Lactate
Lactate (mmol/L)
Duration of Feeding (weeks)

954 **Figure 3. HFD blunted the mitochondrial oxidation of monocyte subsets.** [A-C] Bone marrow cells
955 from mice fed control or HFD for 3, 8 or 18 weeks (n=3 mice per dietary group) were incubated with
956 Mitotracker Red CMXRos for 17 min at 37C. This is a fixable red-fluorescent dye that stains mitochondria
957 dependent on their membrane potential. Cells were then fixed, stained with fluorescent antibodies for flow
958 cytometry, and subjected to fluorescent activated cell sorting (FACS) to identify Ly6C^{low} and Ly6C^{high}
959 monocyte populations. [D-F] Ly6C^{low} and Ly6C^{high} monocytes from mice fed control or HFD for 3, 8 or 18
960 weeks, n=3 mice per dietary group) were isolated via FACS and plated for metabolic analysis of their
961 Oxygen Consumption Rate (OCR) with a Seahorse XF Analyzer. [G-I] Area under the curve of OCR of
962 FACS-sorted Ly6Clow and Ly6Chigh monocytes from control and HFD-fed mice measured by the
963 Seahorse Assay (n=3 mice per dietary group). [J] Area under the curve of ECAR measurement from FACS-
964 sorted Ly6C^{low} and Ly6C^{high} monocytes of control and HFD-fed mice measured by the Seahorse Assay and
965 pooled from all feeding durations. [K] BM lactate measurement of the supernatant fraction in HFD and
966 control samples quantified using a lactate Plus Meter and normalized to the initial volume of BM isolated
967 from the femur. (n=7 mice per dietary group). Results are expressed as mean ± SEM. One-way ANOVA
968 was used for statistical analysis. *$P < 0.05$, **$P < 0.01$ and ns = not significant $P > 0.05$. Graph in panels C
969 was created using FlowJo software (Becton, Dickinson Company).
970

Figure 4

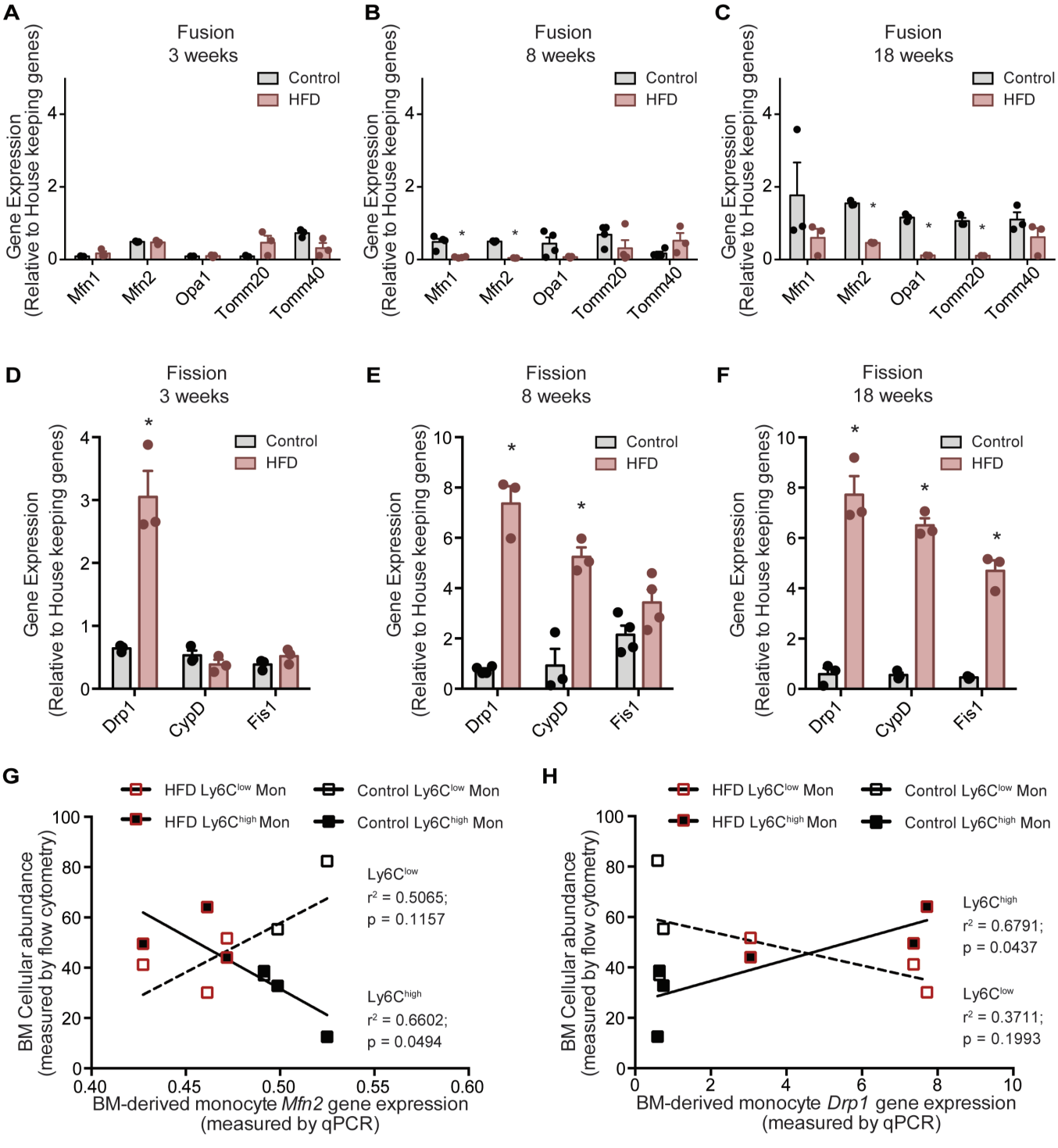
A
Fusion
3 weeks
Control
HFD
Gene Expression
(Relative to House keeping genes)
Mfn1
Mfn2
Opa1
Tomm20
Tomm40
B
Fusion
8 weeks
C
Fusion
18 weeks
D
Fission
3 weeks
Drp1
CypD
Fis1
E
Fission
8 weeks
F
Fission
18 weeks
G
HFD Ly6C^low Mon
Control Ly6C^low Mon
HFD Ly6C^high Mon
Control Ly6C^high Mon
BM Cellular abundance
(measured by flow cytometry)
Ly6C^low
r² = 0.5065;
p = 0.1157
Ly6C^high
r² = 0.6602;
p = 0.0494
BM-derived monocyte Mfn2 gene expression
(measured by qPCR)
H
Ly6C^high
r² = 0.6791;
p = 0.0437
Ly6C^low
r² = 0.3711;
p = 0.1993
BM-derived monocyte Drp1 gene expression
(measured by qPCR)

971 **Figure 4. HFD downregulated expression of mitochondrial fusion genes and upregulated**
972 **mitochondrial fission genes.** Gene expression of mitochondrial fusion genes *Mfn1, Mfn2, Opa1, Tomm20,*
973 and *Tomm40* in monocytes isolated from control and HFD-fed mice for [A] 3, [B] 8, [C] 18 weeks. Gene
974 expression of mitochondrial fission genes *Drp1, CypD* and *Fis1* in monocytes isolated from control and
975 HFD-fed mice for [D] 3, [E] 8, [F] 18 weeks. (n=3 mice per dietary group and samples were analyzed in
976 duplicates). [G] Correlative analysis of monocyte subset BM cellular abundance and BM-derived monocyte
977 *Mfn2* gene expression. [H] Correlative analysis of the average of monocyte subset BM cellular abundance
978 (n=8 per dietary group) and BM-derived monocyte *Drp1* gene expression (n=3 per dietary group) per
979 dietary group at each time point. Correlative analysis statistics were conducted using the linear regression
980 analysis testing whether slopes and intercepts are significantly different via GraphPad Prism version 6
981 (GraphPad Software). The r^2 represents the goodness of the fit while the P values greater than 0.05 represent
982 whether the slope of the line of best fit is significantly non-zero. Results are expressed as mean ± SEM.
983 One-way ANOVA was used for statistical analysis. *$P < 0.05$ and ns = not significant $P > 0.05$.

984

Figure 5

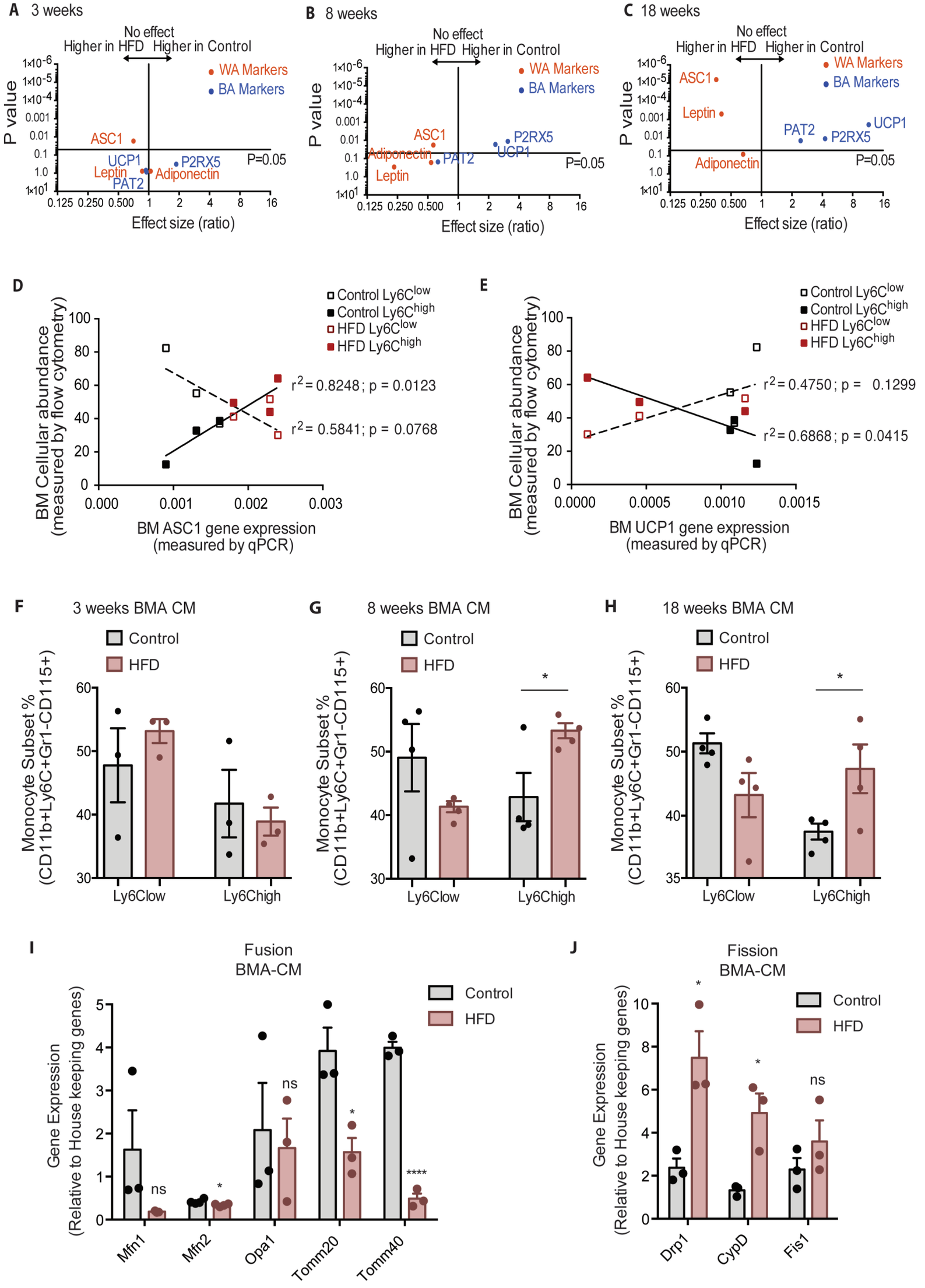
A 3 weeks
B 8 weeks
C 18 weeks
No effect
Higher in HFD
Higher in Control
WA Markers
BA Markers
P value
Effect size (ratio)
P=0.05
ASC1
UCP1
P2RX5
Leptin
Adiponectin
PAT2
D
E
Control Ly6C^low
Control Ly6C^high
HFD Ly6C^low
HFD Ly6C^high
BM Cellular abundance (measured by flow cytometry)
BM ASC1 gene expression (measured by qPCR)
BM UCP1 gene expression (measured by qPCR)
r^2 = 0.8248 ; p = 0.0123
r^2 = 0.5841; p = 0.0768
r^2 = 0.4750 ; p = 0.1299
r^2 = 0.6868 ; p = 0.0415
F 3 weeks BMA CM
G 8 weeks BMA CM
H 18 weeks BMA CM
Control
HFD
Monocyte Subset % (CD11b+Ly6C+Gr1-CD115+)
Ly6Clow
Ly6Chigh
I Fusion BMA-CM
J Fission BMA-CM
Gene Expression (Relative to House keeping genes)
Mfn1
Mfn2
Opa1
Tomm20
Tomm40
Drp1
CypD
Fis1
ns
*
****

985 **Figure 5. Bone marrow adipocyte whitening detected at 8 and 18 weeks of HFD favours increased**
986 **bone marrow Ly6C^{high} monocytes and induced changes in mitochondrial dynamic gene expression.**
987 Volcano plots showing the gene expression of white and brown adipocyte markers in red and blue
988 respectively [A] at 3, [B] 8 and [C] 18 weeks of HFD (n=3-9 per dietary group). Correlative graphs of the
989 [D] white adipocyte marker ASC1 (n=8-9 per dietary group) and [E] brown adipocyte marker UCP1 (n=6
990 per dietary group) with Ly6Clow or Ly6Chigh monocyte subset abundance in the BM (n=8). Correlative
991 analysis statistics were conducted using the linear regression analysis testing whether slopes and intercepts
992 are significantly different via GraphPad Prism version 6 (GraphPad Software). The r^2 represents the
993 goodness of the fit while the P values greater than 0.05 represent whether the slope of the line of best fit is
994 significantly non-zero. [F-H] Flow cytometry quantification of naïve Ly6C^{low} and Ly6C^{high} monocytes
995 (n=3-4 per dietary group) from *in vitro*-generated monocytes pre-treated for 18 h with pooled BMA-CM
996 collected from three mice fed the control and HFD for 3, 8 and 18 weeks. [I] Gene expression of
997 mitochondrial fusion genes *Mfn1, Mfn2, Opa1, Tomm20,* and *Tomm40* in naïve monocytes treated with
998 BMA-CM from control and HFD-fed mice (n=3 per dietary group and samples were run in duplicates). [J]
999 Gene expression of mitochondrial fission genes *Drp1, CypD* and *Fis1* in naïve monocytes treated with
1000 BMA-CM from control and HFD-fed mice (n=3 per dietary group and samples were run in duplicates).
1001 Results are expressed as mean ± SEM. One-way ANOVA was used for statistical analysis at each dietary
1002 group and across feeding periods. *P < 0.05, ****P < 0.0001 and ns = not significant > 0.05.

1003

Figure 6

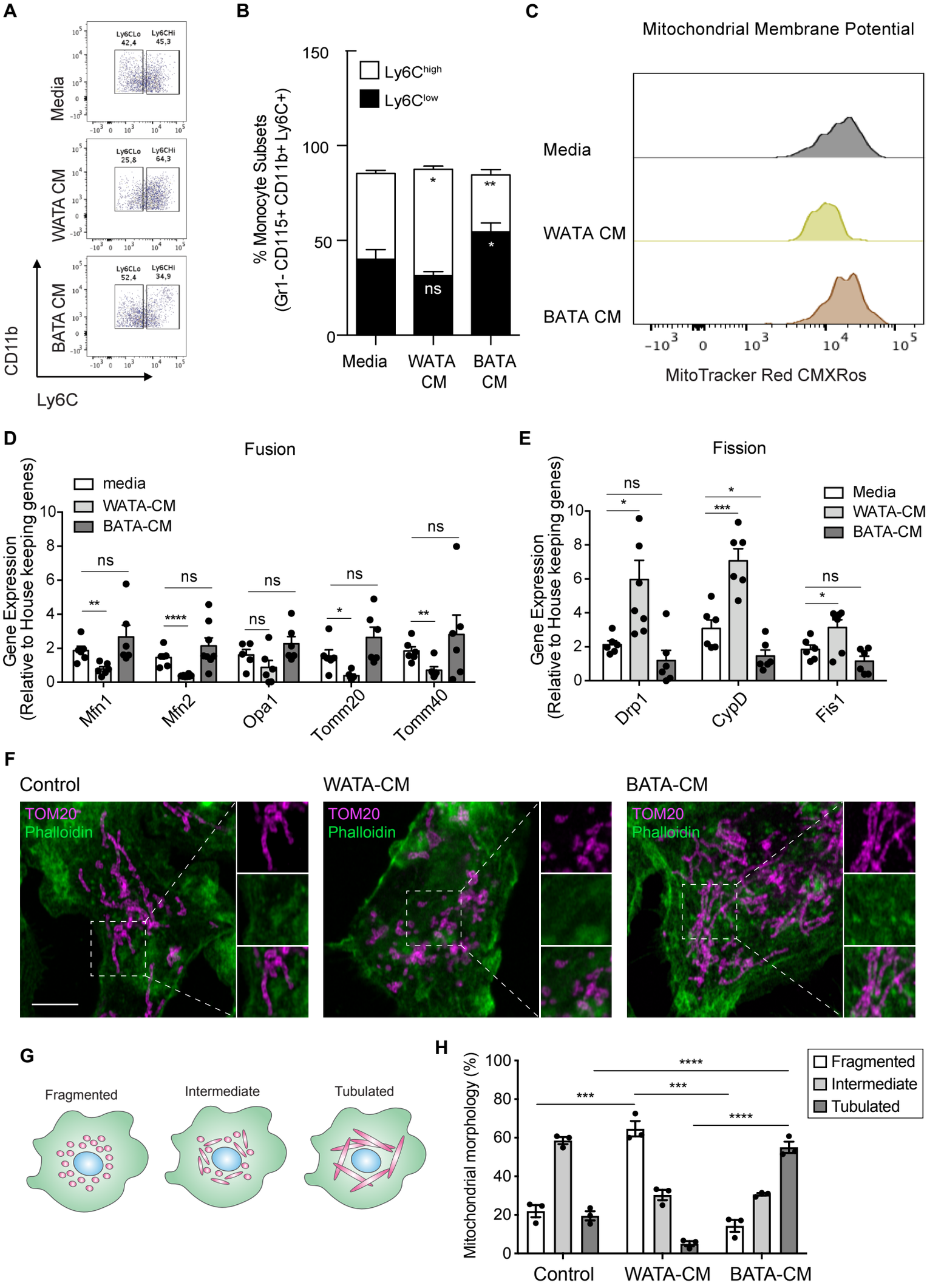
A
Media
WATA CM
BATA CM
Ly6CLo 42,4
Ly6CHi 45,3
Ly6CLo 25,8
Ly6CHi 64,3
Ly6CLo 52,4
Ly6CHi 34,9
CD11b
Ly6C
B
Ly6C^high
Ly6C^low
% Monocyte Subsets (Gr1- CD115+ CD11b+ Ly6C+)
Media
WATA CM
BATA CM
ns
C
Mitochondrial Membrane Potential
Media
WATA CM
BATA CM
MitoTracker Red CMXRos
D
Fusion
media
WATA-CM
BATA-CM
Gene Expression (Relative to House keeping genes)
Mfn1
Mfn2
Opa1
Tomm20
Tomm40
E
Fission
Media
WATA-CM
BATA-CM
Gene Expression (Relative to House keeping genes)
Drp1
CypD
Fis1
F
Control
WATA-CM
BATA-CM
TOM20
Phalloidin
G
Fragmented
Intermediate
Tubulated
H
Mitochondrial morphology (%)
Fragmented
Intermediate
Tubulated
Control
WATA-CM
BATA-CM

1004 **Figure 6. *Bona fide* white adipocytes favoured Ly6C^{high} monocytes preponderance, blunted monocyte**
1005 **mitochondrial membrane potential, and induced mitochondrial fragmentation *in vitro*.** Naïve BM-
1006 derived monocytes were treated with CM from isolated *bone fide* white and brown adipocytes from EWAT
1007 and inter-scapular BAT for 18 h. [A] Flow cytometry dot plots detecting the effects of 18 h of treatment
1008 with media alone, pooled WATA-CM and BATA-CM from three mice (n=3 technical replicates each time
1009 with pooled CM from 3 mice) on monocyte subset abundance. [B] quantification of the gates drawn for
1010 Ly6C^{low} and Ly6C^{high} monocytes. (n=9 biological replicates from naïve monocytes treated). [C]
1011 Representative plot of MitoTracker Red CMXRos detected by flow cytometry in Ly6C^{low} monocytes
1012 treated with media alone, pooled WATA-CM and BATA-CM for 18 h. [D] Gene expression of
1013 mitochondrial fusion genes *Mfn1*, *Mfn2*, *Opa1*, *Tomm20*, and *Tomm40* in naïve BM-derived monocytes
1014 treated with control Media, pooled WATA-CM and BATA-CM. (n=6 mice in each CM group and samples
1015 were analyzed in duplicates). [E] Gene expression of mitochondrial fission genes *Drp1*, *CypD* and *Fis1* in
1016 naïve BM-derived monocytes treated with control Media, WATA-CM and BATA-CM. (n=6 mice in each
1017 CM group and samples were analyzed in duplicates). Results in [B], [D] and [E] are expressed as mean ±
1018 SEM, with one-way ANOVA used for statistical analysis: *P < 0.05, **P < 0.01 and ***P < 0.001, ****P
1019 < 0.0001 and ns = not significant P > 0.05. Graphs in [A] and [C] were created using FlowJo software
1020 (Becton, Dickinson Company). [F] Super-resolution microscopy images of mitochondrial morphology via
1021 TOM20 staining in BM-derived monocytes treated with control Media, pooled WATA-CM and BATA-
1022 CM (representative of n=3 mice in each CM group). Scale bar = 5μm. Images were analyzed in Fiji (version
1023 2.1.0/1.53c). [G] Schematic illustration of mitochondrial morphologies as fragmented, intermediate, or
1024 tubulated. [H] Quantification of the percentage of monocytes with the indicated mitochondrial morphology,
1025 in each treatment condition. Values are from three independent experiments; n=3 mice in each CM group;
1026 about 40 cells counted for each condition, within each experiment. Results are expressed as mean ± SEM.
1027 One-way ANOVA was used for statistical analysis. *P < 0.05, **P < 0.01 and ***P < 0.001, ****P <
1028 0.0001 and ns = not significant P > 0.05.

Figure 7

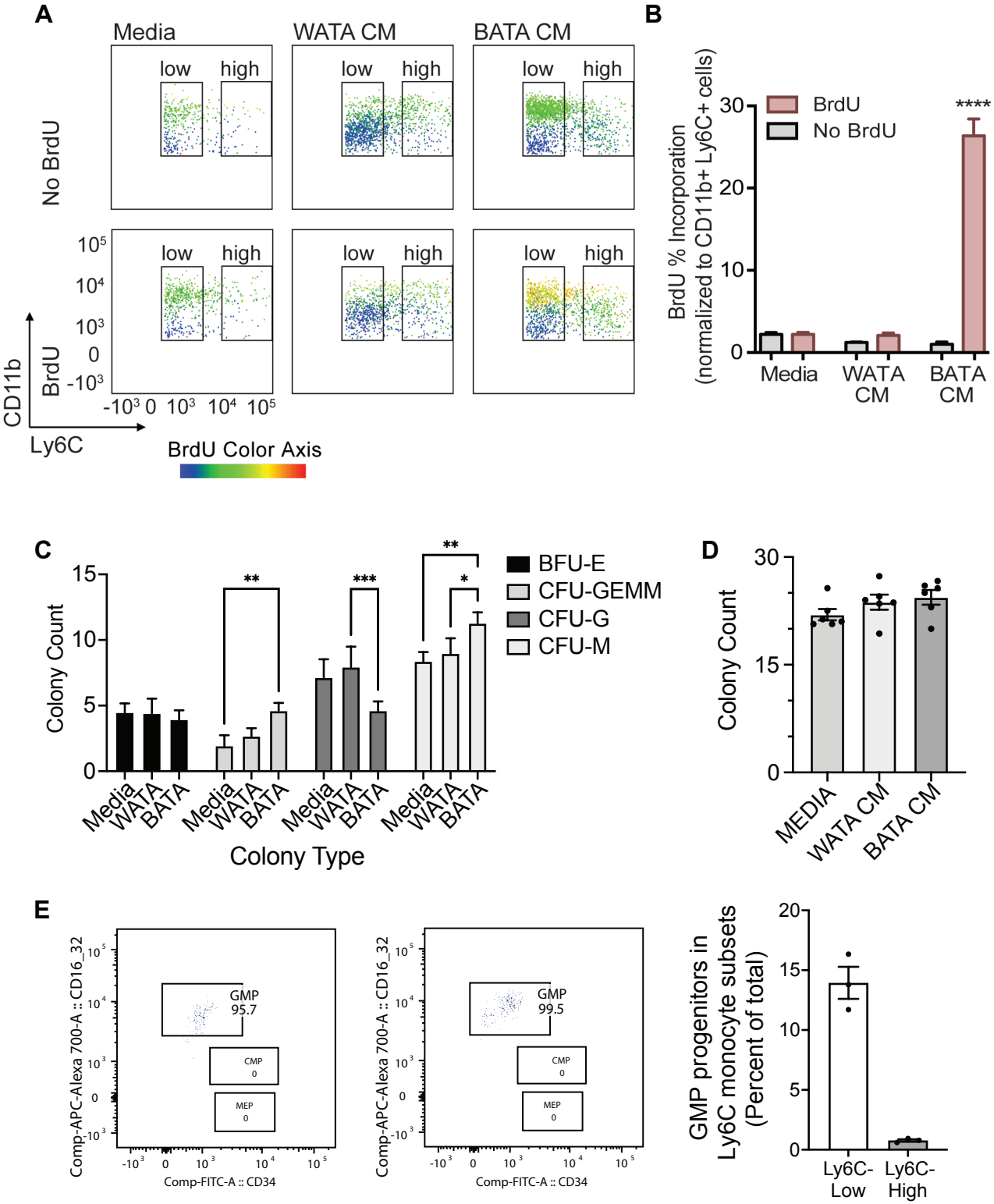
A
Media
WATA CM
BATA CM
low
high
No BrdU
BrdU
CD11b
Ly6C
BrdU Color Axis
B
BrdU
No BrdU
BrdU % Incorporation
(normalized to CD11b+ Ly6C+ cells)
****
Media
WATA CM
BATA CM
C
Colony Count
Colony Type
BFU-E
CFU-GEMM
CFU-G
CFU-M
D
Colony Count
MEDIA
WATA CM
BATA CM
E
Comp-APC-Alexa 700-A :: CD16_32
Comp-FITC-A :: CD34
GMP
95.7
99.5
CMP
MEP
GMP progenitors in
Ly6C monocyte subsets
(Percent of total)
Ly6C-
Low
Ly6C-
High

1029 **Figure 7. Brown adipocytes favour Ly6C^{low} monocytes through progenitor cell differentiation and**
1030 **proliferation.** [A] BM-derived, *in vitro*-generated monocytes were treated with media alone, WATA-CM
1031 or BATA-CM in the presence of the pyrimidine analogue BrdU to detect cellular proliferation. [B]
1032 Quantification of BrdU abundance in Ly6C^{low} and Ly6C^{high} monocyte subsets with the treatments in panel
1033 A, was determined by flow analysis (yellow to red signal, see Methods). Results are expressed as mean ±
1034 SEM, n=3-6 individual mice per group. One-way ANOVA test was used for statistical analysis, ****$p <$
1035 0.0005. [C, D] Colony Forming Unit assays were performed as described in Methods using six independent
1036 cultures of BM-derived, *in vitro*-generated monocytes, (n=6 individual mice), were treated with WATA-
1037 CM, BATA-CM or control adipocyte media (Media) for 18 h prior to mixing with methylcellulose-based
1038 media and plating at 20,000 cells/ml to 6-well plates, in triplicate. [C] BATA-CM promoted CFU-GEMM
1039 cultures over Media alone (**$p<0.01$ Two-way ANOVA, Tukey's multiple comparisons) and tilting
1040 granulocyte/macrophage progenitors towards macrophage (CFU-M) over granulocyte (CFU-G)
1041 differentiation, relative to Media alone (**$p<0.01$) or WATA-CM (*$p<0.05$ or ***$p<0.001$). [D] The counts
1042 of the different colonies for each treatment (Media, WATA-CM or BATA-CM) were totaled and plotted as
1043 the mean ± SEM (n=6 individual mice). There was no statistical difference between the media treatments.
1044 [E] Isolated BM cells were processed for flow analysis to determine the progenitor cell populations present
1045 in the Ly6C^{low} or Ly6C^{high} monocyte subsets. The percent GMP ratio was calculated relative to the total
1046 cells detected in either monocyte subset as the mean ± SEM (isolated from n=3 individual mice). Graphs
1047 in panel A were created using FlowJo software (Becton, Dickinson Company).

1048

Figure 8

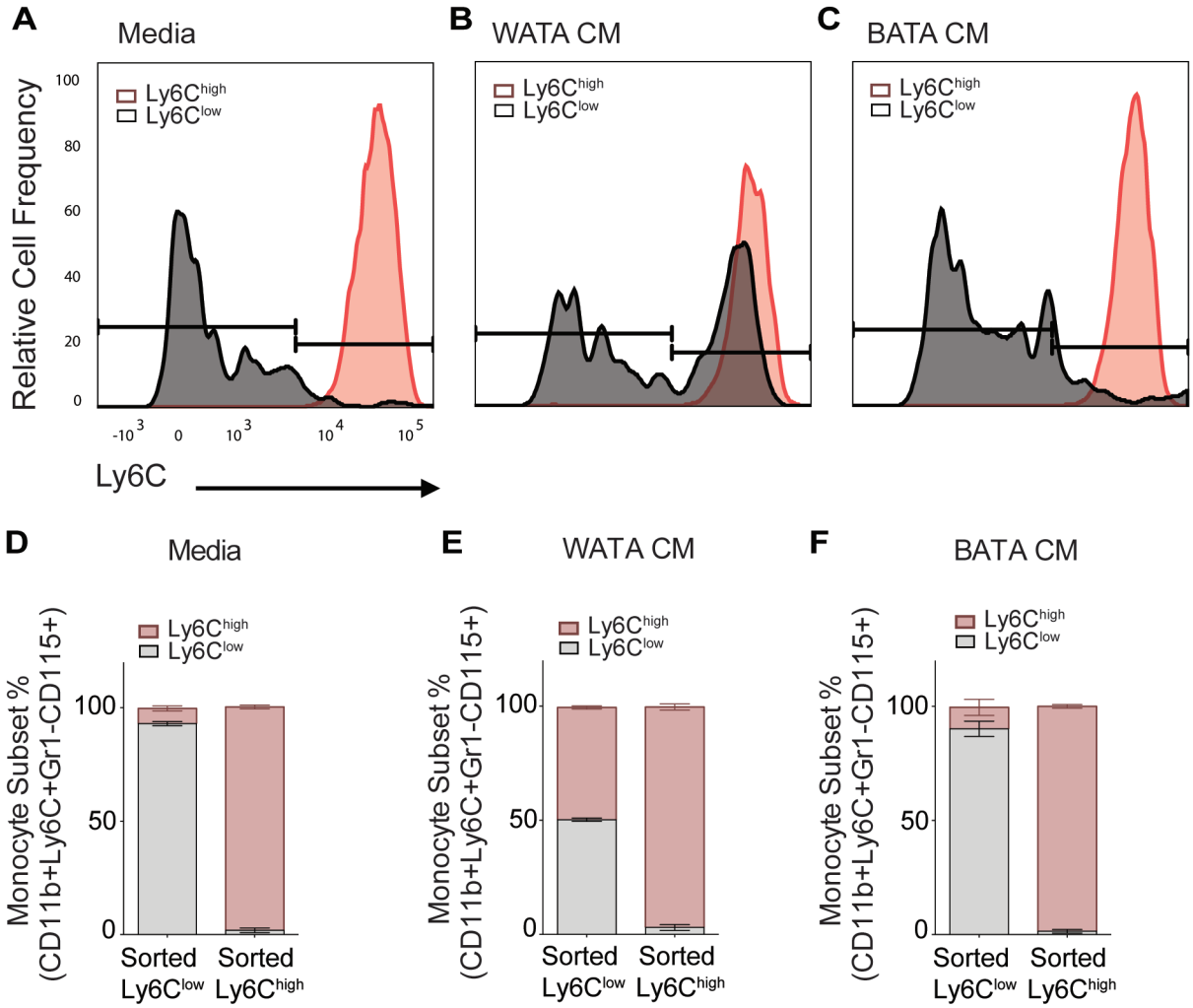
A
Media
B
WATA CM
C
BATA CM
Relative Cell Frequency
100
80
60
40
20
0
Ly6C^high
Ly6C^low
-10^3
0
10^3
10^4
10^5
Ly6C
D
Media
E
WATA CM
F
BATA CM
Monocyte Subset %
(CD11b+Ly6C+Gr1-CD115+)
100
50
0
Sorted Ly6C^low
Sorted Ly6C^high

1049 **Figure 8. WATA-CM tilts BM-derived Ly6C^{low} monocytes towards Ly6C^{high} monocytes.**
1050 Representative plots of FACS-sorted Ly6C^{low} (gray) and Ly6C^{high} (red) monocytes from control mice were
1051 independently treated with [A] Media alone, [B] WATA-CM, or [C] BATA-CM (n=6 mice per FACS-
1052 sorted monocyte group) for 18 h after which the presence of the alternate monocyte subset was assessed
1053 via flow cytometry. [D-F] Quantification of Ly6C^{low} and Ly6C^{high} gates in panels A-C. [G] BM-derived, *in*
1054 *vitro*-generated monocytes were analyzed for gene expression of the Ly6C^{low} marker SPN and the Ly6C^{high}
1055 marker Ly6C2 by qPCR as described in the Methods.

1056 Graphs in panels A-C were created using FlowJo software (Becton, Dickinson Company).

1057

Figure S1

A

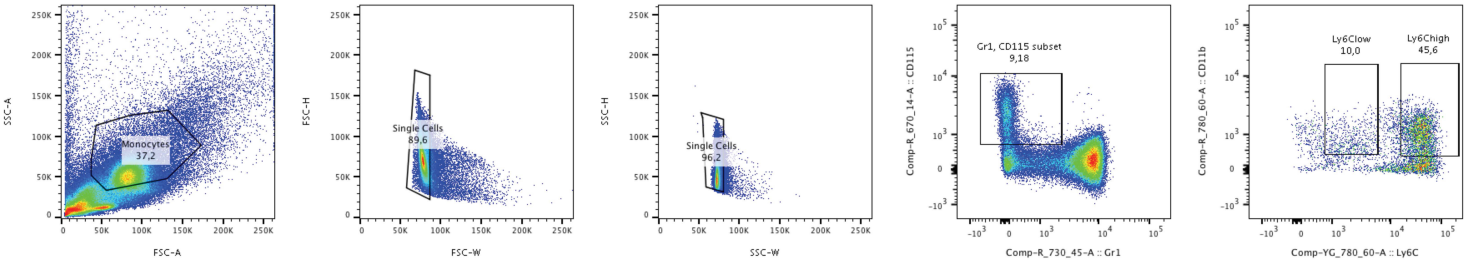

B

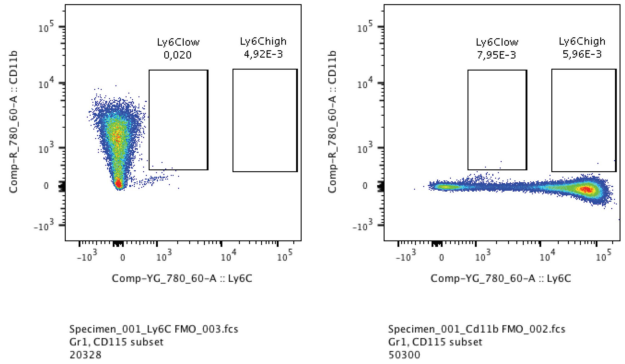

C

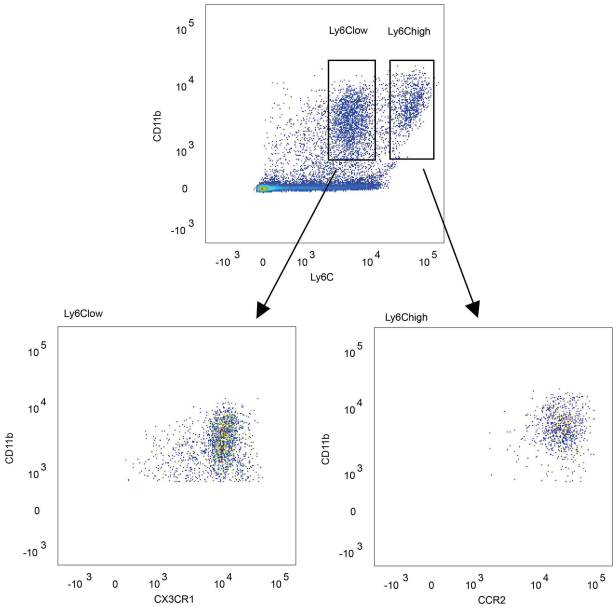

D

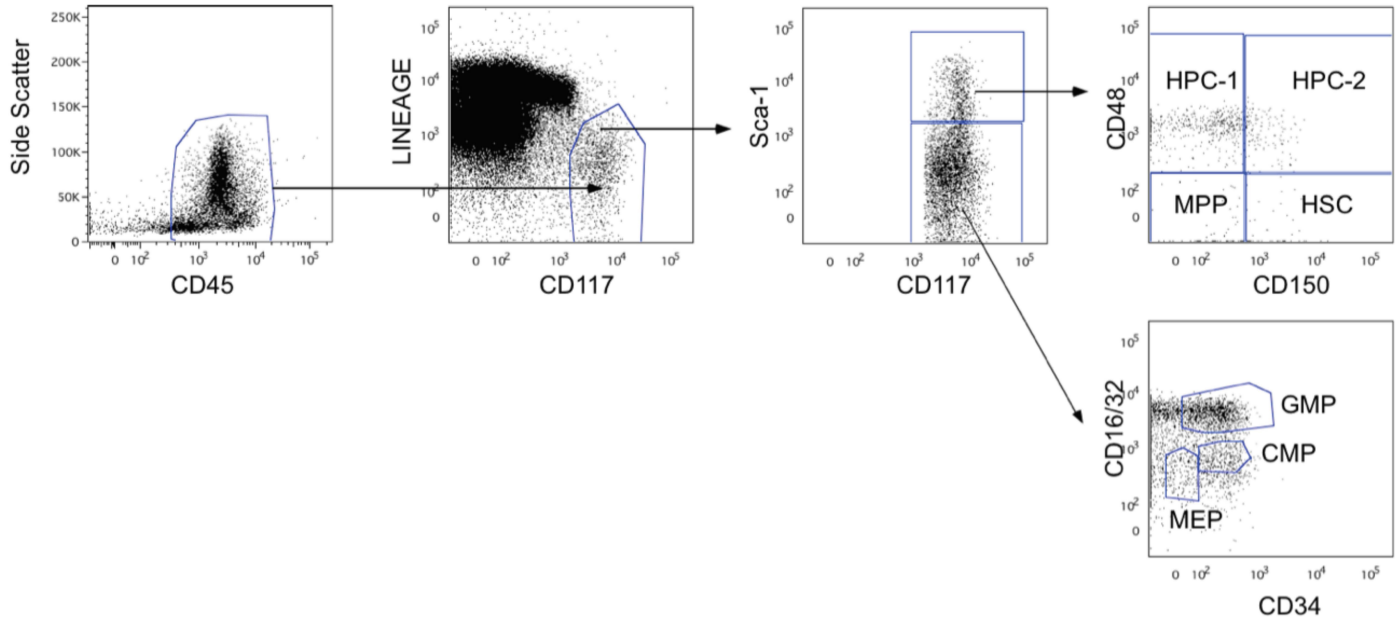

1058 **SUPPLEMENTAL MATERIAL**

1059 **Figure S1: Flow cytometry gating strategy for identification of Ly6C^{low} and Ly6C^{high} monocytes and**
1060 **their progenitor cells.** Following red blood cell lysis, SVF, blood and the BM were washed with FACS
1061 buffer (PBS, 1% (v/v) heat-inactivated FBS, 0.2% (w/v) BSA), stained with Aqua Live/Dead Antibody
1062 (ThermoFisher, L34957) for 15 min in the dark, washed with FACS buffer again, blocked with anti-mouse
1063 CD16/32 antibody (eBioscience, 14-0161-86) for 15 min in the dark following a 30 min incubation with
1064 the indicated antibodies. [A] Using side and forward scatter to identify singlet cells, CD115+Gr1- cells
1065 were identified that were further analyzed using CD11b and Ly6C. [B] Ly6C^{low} and Ly6C^{high} monocyte
1066 gates were drawn using fluorescence minus one (FMO) controls for CD11b and Ly6C. [C] The subsets
1067 were further confirmed via CX3CR1 and CCR2, respectively. [D] CD45+ cells were analyzed using a
1068 lineage cocktail of antibodies (**Table 1**) and CD117+, further broken down into Sca1+ and – cells. Sca1+
1069 cells were further classified using CD48 and CD150 while Sca1- cells were further characterized via
1070 CD16/32 and CD34. Graphs were created using FlowJo software (Becton, Dickinson Company).

1071

Figure S2

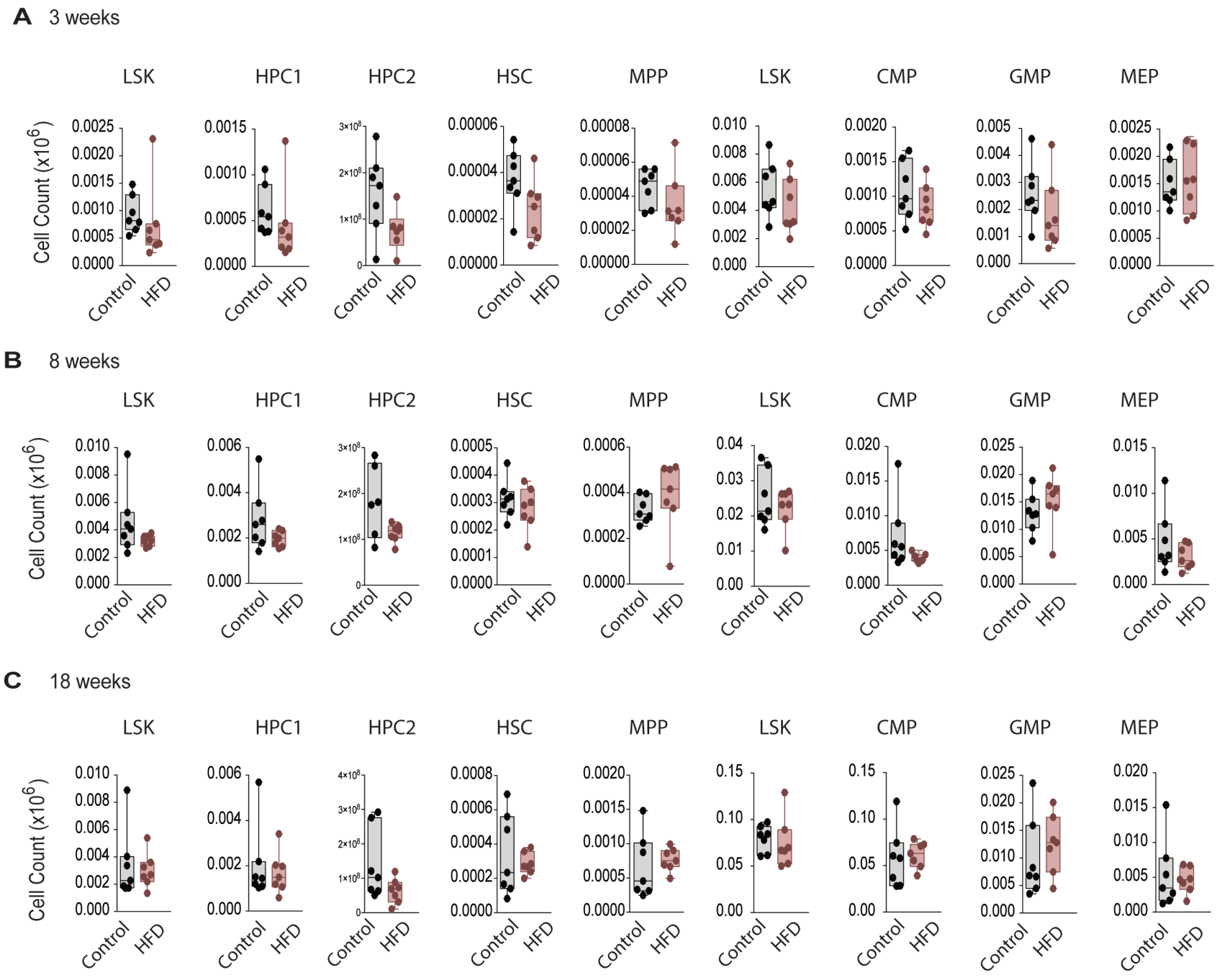
A 3 weeks
B 8 weeks
C 18 weeks
LSK
HPC1
HPC2
HSC
MPP
LSK
CMP
GMP
MEP
Cell Count (x10^6)
Control
HFD

1072 **Figure S2. Monocyte progenitors and stem cells were not significantly altered with HFD *in vivo*.** Flow
1073 cytometry analysis of HSC and monocyte progenitor cells in mice fed a Control or HFD for [A] 3, [B] 8,
1074 and [C] 18 weeks. (n = 6-7 per dietary group at each feeding duration) Flow cytometry antibodies used are
1075 listed in Table 1. Student's T test was used and no statistical significance was observed (ns = not significant
1076 > 0.05).

1077

Figure S3

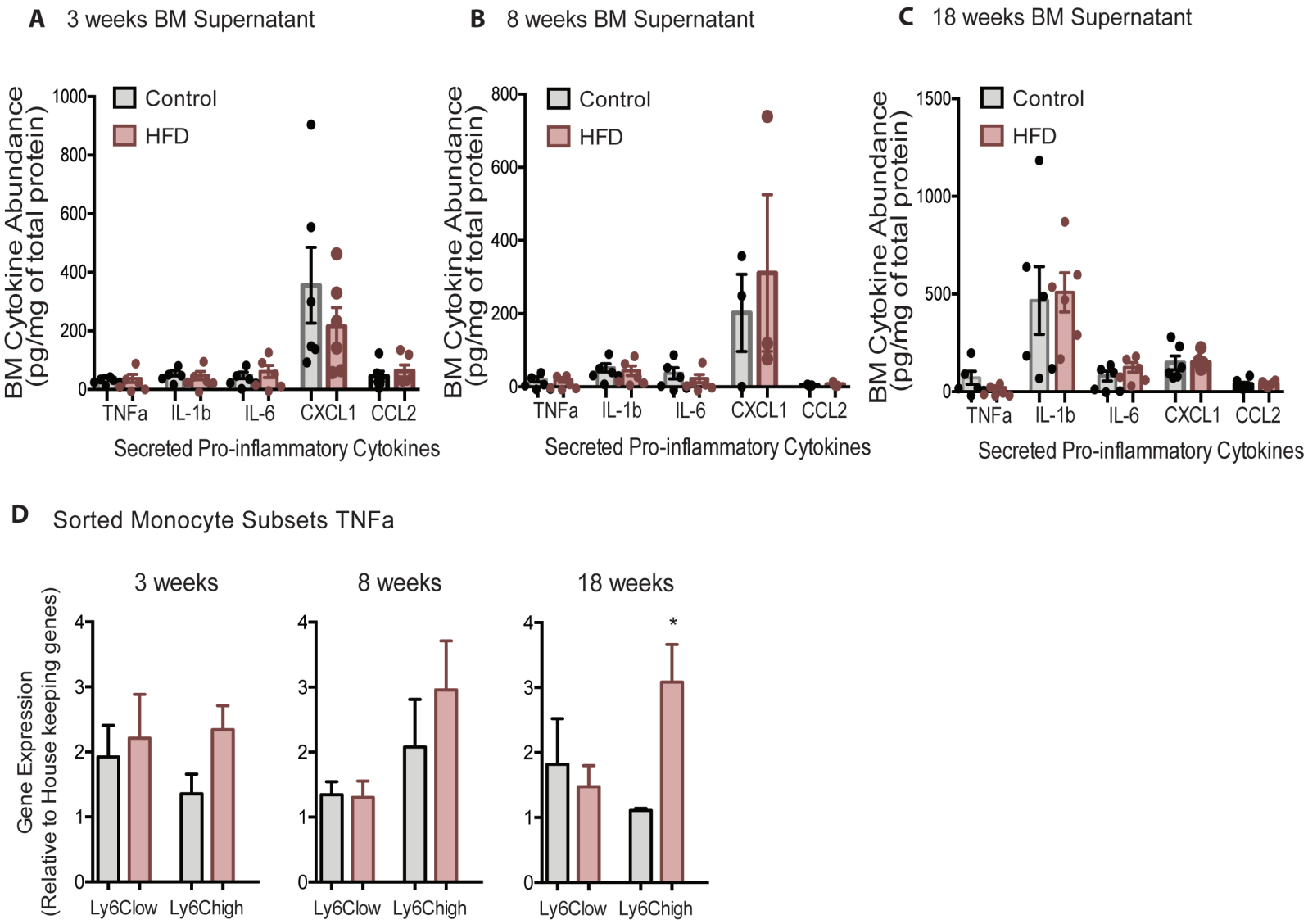
A 3 weeks BM Supernatant
B 8 weeks BM Supernatant
C 18 weeks BM Supernatant
Control
HFD
BM Cytokine Abundance (pg/mg of total protein)
TNFa
IL-1b
IL-6
CXCL1
CCL2
Secreted Pro-inflammatory Cytokines
D Sorted Monocyte Subsets TNFa
3 weeks
8 weeks
18 weeks
Gene Expression (Relative to House keeping genes)
Ly6Clow
Ly6Chigh
*

1078 **Figure S3: BM pro-inflammatory factors did not change with HFD.** No changes in pro-inflammatory
1079 cytokines were detected in BM supernatant fraction using the ELISA assay in mice fed control or HFD for
1080 [A] 3, [B] 8, or [C] 18 weeks. (n = 3-6 mice in each dietary group at feeding duration) [D] FACS-sorted
1081 monocyte subsets were analyzed for changes in pro-inflammatory gene expression; shown in TNFα gene
1082 expression increased with 18 weeks of HFD in Ly6C^{high} monocytes, but no other changes were detected. (n
1083 = 3 mice in each dietary group at each feeding duration) Results are expressed as mean ± SEM. One way
1084 ANOVA test was used for statistical analysis. *P < 0.05, **P < 0.01 and ns = not significant P > 0.05.

1085

Figure S4

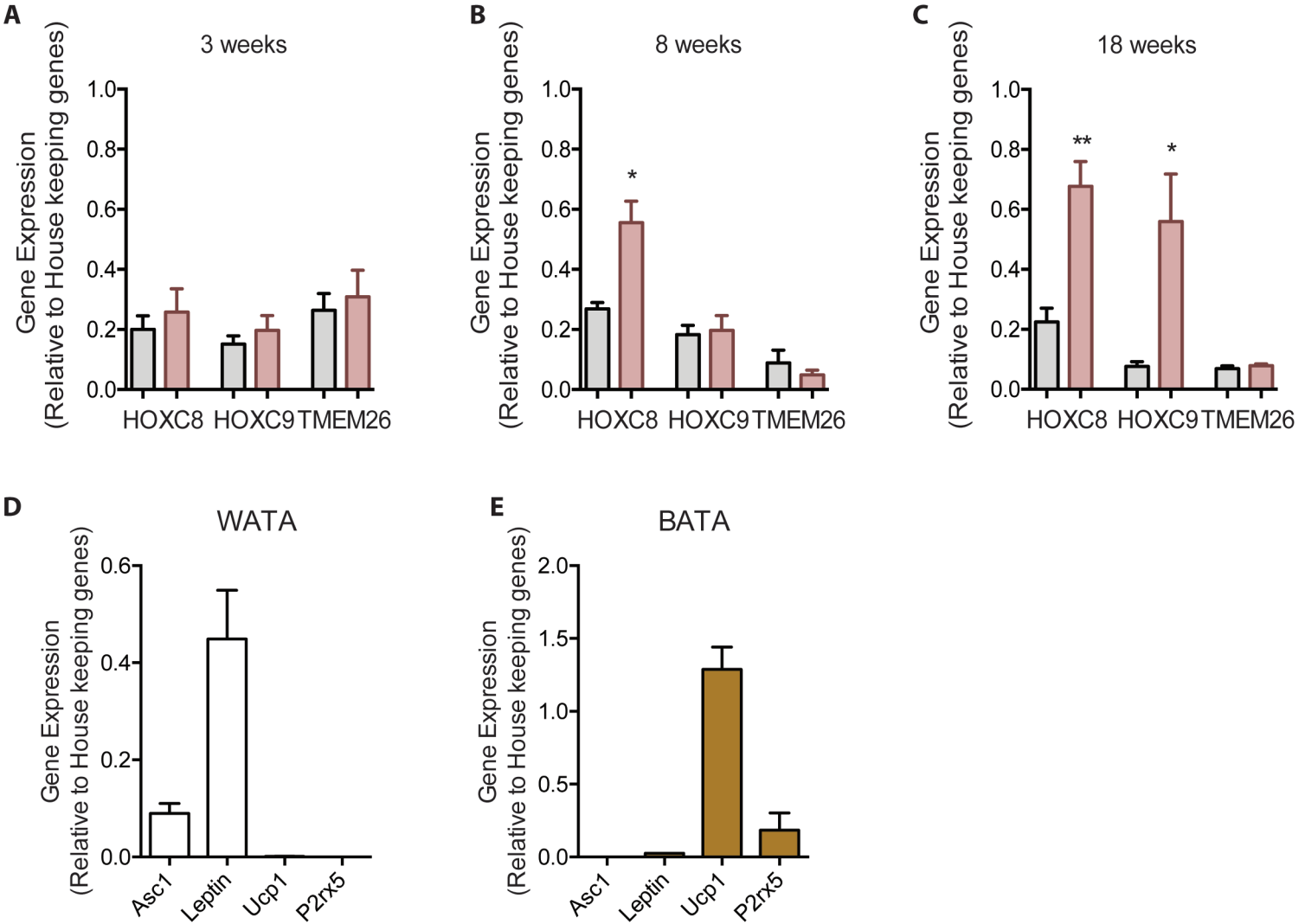
A
3 weeks
Gene Expression
(Relative to House keeping genes)
1.0
0.8
0.6
0.4
0.2
0.0
HOXC8
HOXC9
TMEM26
B
8 weeks
*
C
18 weeks
**
*
D
WATA
0.6
0.4
0.2
0.0
Asc1
Leptin
Ucp1
P2rx5
E
BATA
2.0
1.5
1.0
0.5
0.0

1086 **Figure S4. BMA precursor cells with HFD.** RT qPCR of isolated pelleted fraction were assessed for pre-
1087 adipocyte markers of mice fed a Control or HFD for [A] 3, [B] 8, and [C] 18 weeks. (n=3 mice per dietary
1088 group and samples were analyzed in duplicates). Results are expressed as mean ± SEM. One way ANOVA
1089 test was used for statistical analysis. *$P < 0.05$, **$P < 0.01$ and ns = not significant $P > 0.05$. [D] classical
1090 white and brown adipocyte markers were confirmed in isolated WATA and BATA. (n=2 mice per tissue
1091 and samples were analyzed in duplicates) No statistical analysis was conducted on data presented in panel
1092 D as the brown adipocyte genes were undetectable in WATA and vice versa.

1093

1094

Figure S5

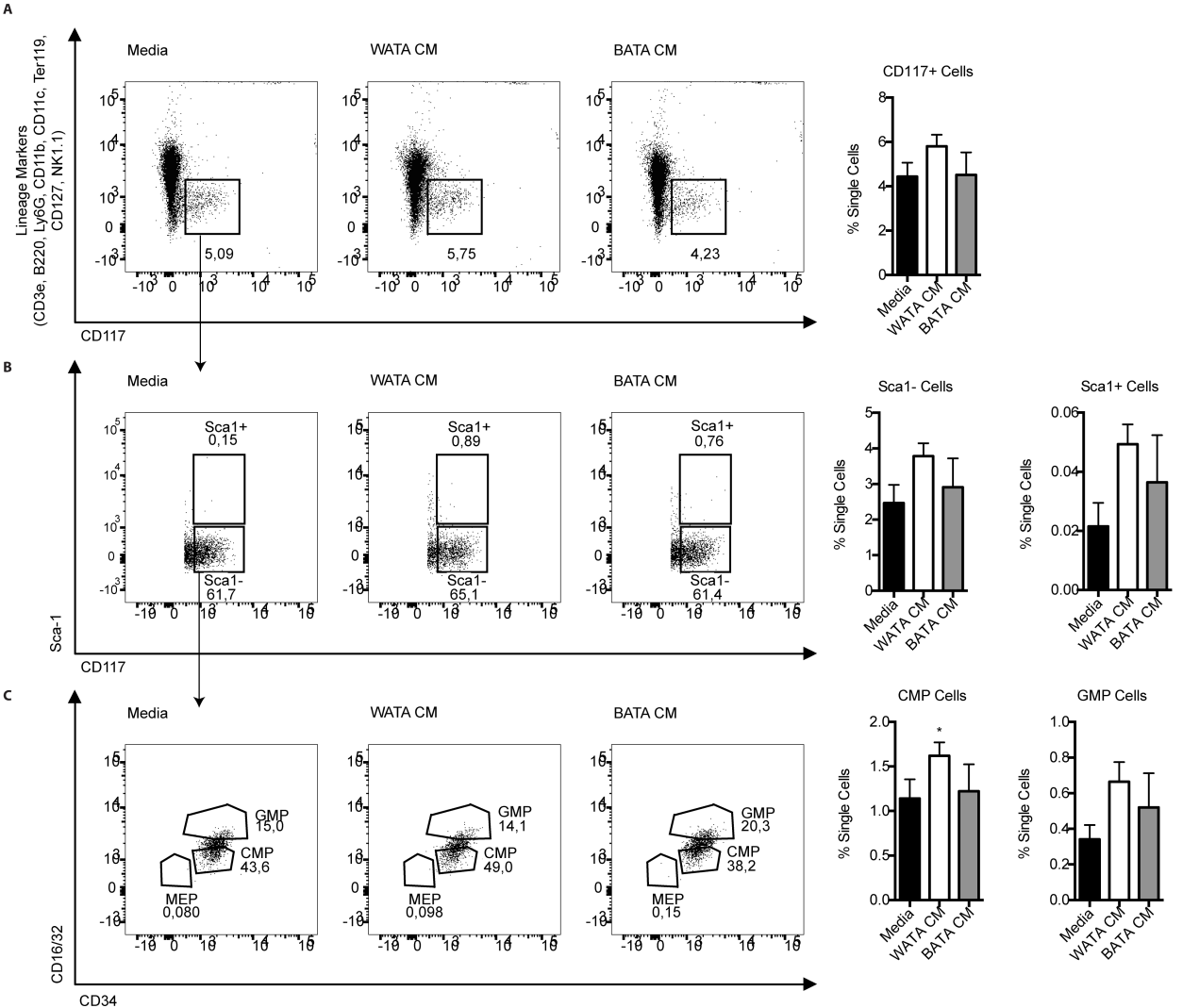
A
Lineage Markers
(CD3e, B220, Ly6G, CD11b, CD11c, Ter119, CD127, NK1.1)
CD117
Media
WATA CM
BATA CM
5,09
5,75
4,23
CD117+ Cells
% Single Cells
B
Sca-1
Sca1+
0,15
0,89
0,76
Sca1-
61,7
65,1
61,4
Sca1- Cells
Sca1+ Cells
C
CD16/32
CD34
GMP
15,0
14,1
20,3
CMP
43,6
49,0
38,2
MEP
0,080
0,098
0,15
CMP Cells
GMP Cells

1095 **Figure S5: HSC and their progenitors following the white and brown CM treatment for 18 h.** [A-C]
1096 Flow cytometry analysis was used to test for the presence and changes in HSC and monocyte progenitor
1097 cells in BM-derived, *in vitro*-generated BM-derived monocytes treated with media, WATA-CM, and
1098 BATA-CM. Flow cytometry antibodies used are listed in Table 1 (n=3 individual mice per CM group). One
1099 way ANOVA test was used for statistical analysis. *$P < 0.05$ and ns = not significant $P > 0.05$.
1100

Figure S6

A

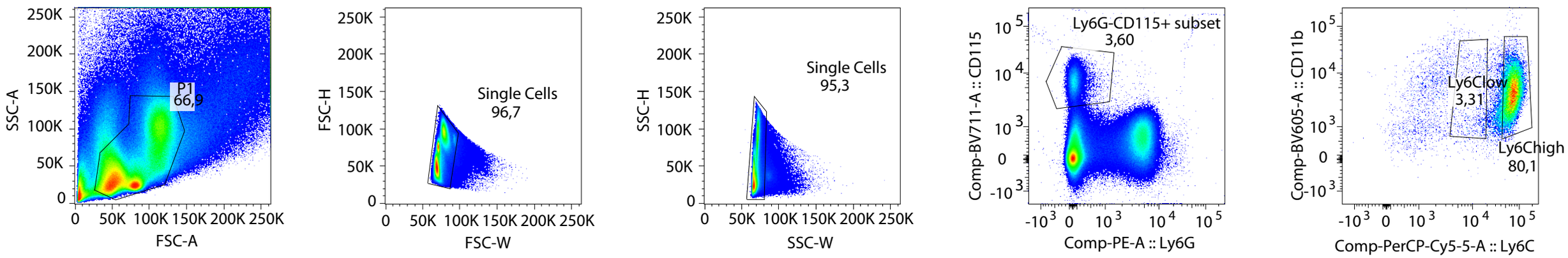

B

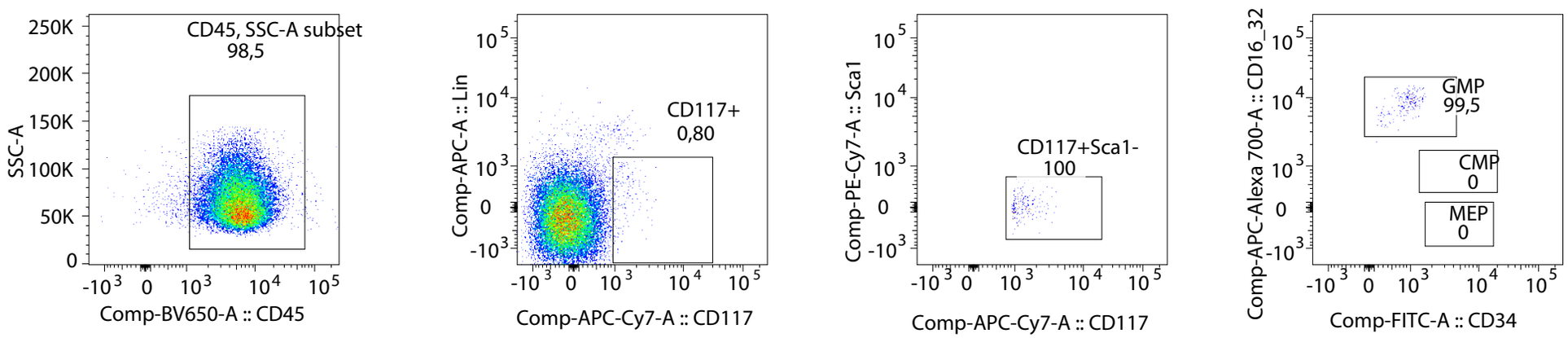

C

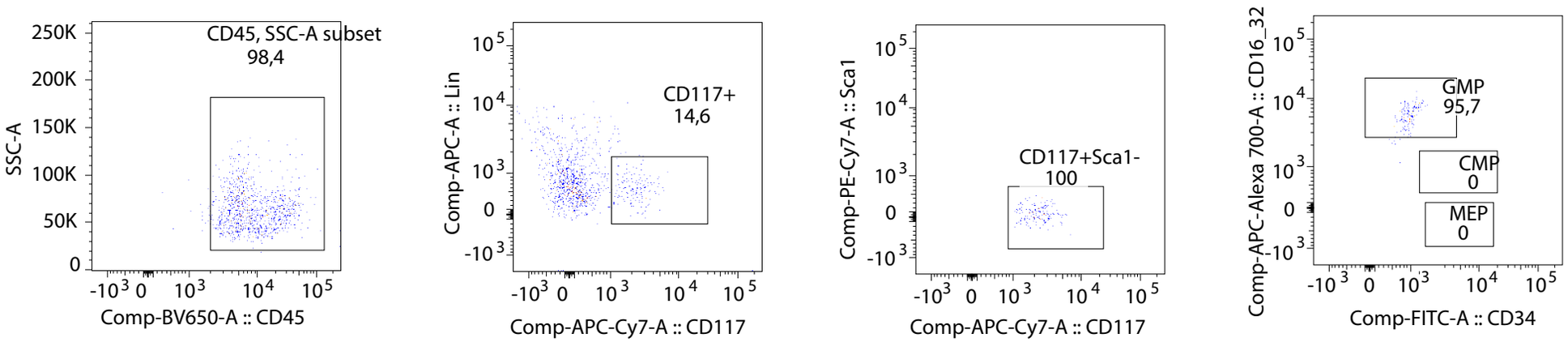

1101 **Figure S6: Flow cytometry gating strategy for identification of progenitor cells within Ly6C^{low} and**
1102 **Ly6C^{high} monocyte subsets.** To prevent contamination of blood in BM cells, mice (n=3 individual mice)
1103 were placed under deep anesthesia using isoflurane and underwent intra-cardiac perfusion with 10 mL of
1104 cold PBS, before sacrifice. Femurs were surgically removed and crushed with a mortar and pestle and bone
1105 marrow cells suspended in PBS were filtered through a 40-µm-nylon mesh. Cells were pelleted at 300 × g,
1106 5 min and resuspended in 500 µl FACS Buffer. 100 µl was aliquoted and stained with the antibody cocktail
1107 for 30 min. Antibodies for CD117, CD16/32 and CD34, were used at 1:50 dilution, all others at 1:100
1108 dilution. Samples were fixed (BD, Cytofix) before being run on a BD LSR Fortessa cytometer. [A] Gating
1109 strategy for Ly6C^{low} and Ly6C^{high}. [B] Gating strategy for progenitor cell identification in the Ly6C^{high}
1110 monocytes. [C] Gating strategy for progenitor cell identification in the Ly6C^{low} monocytes.
1111

1112 **Table 1. List of Antibodies used for flow cytometry analysis.**

Markers	Fluorophore	Manufacturer	Clone	Catalog Number
CD11b	APC-eFluor 780	eBioscience	M1/70	47-0112-82
Ly6C	PE-Cy7	Biolegend	HK1.4	128018
Gr-1	Alexa Fluor 700	eBioscience	RB6-8C5	56-5931-82
CX3CR1	Brilliant Violet 421	Biolegend	SA011F11	149023
CCR2	Alexa594	R&D Systems	475301	FAB5538T
CD115	APC	eBioscience	AFS98	17-1152-82
F4/80	PerCP-Cy5.5	BioLegend	BM8	123128
CD11c	FITC	eBioscience	N418	11-0114-81
CD34	FITC	BD Biosciences	RA1434	553733
CD16/32	APC-R700	BD Biosciences	2.4G2	565502
CD45.2	BV650	BD Biosciences	30-F11	563410
CD150	PEPCP710	invitrogen	mShad150	46-1502-82
CD117	APC/Fire 750	BioLegend	2B8	105838
SCA1	PE-Cy7	Invitrogen	D7	25-5981-82
CD48	BV605	BioLegend	MM48-1	103441
CD3e*	PE	BD Biosciences	17A2	555725
B220*	PE	BD Biosciences	RA3-6B2	553089
Ly6G*	PE	BD Biosciences	1A8	551461
CD11b*	PE	BD Biosciences	M1/70	553311
CD11c*	PE	BioLegend	N418	117308
Ter119*	PE	BD Biosciences	TER-119	553623
CD127*	PE	eBioscience	A7R34	12-1271-82
NK1.1*	PE	BD Biosciences	PK138	553165

1113 *LINEAGE is a cocktail of antibodies containing CD3e, B220, Ly6G, CD11b, CD11c, Ter119, CD127,
1114 NK1.1 with the same fluorophore to exclude all terminally differentiated cells.